

Efficient cluster expansion for substitutional systems

David B. Laks, L. G. Ferreira, Sverre Froyen, and Alex Zunger

National Renewable Energy Laboratory, Golden, Colorado 80401

(Received 2 June 1992)

We demonstrate a cluster expansion technique that is capable of accurately predicting formation energies in binary substitutional systems—even for those with large atomic relaxations. Conventional cluster expansions converge rapidly only in the absence of atomic relaxations, and they fail for long-period lattice-mismatched superlattices. When combined with first-principles total-energy methods, our method allows for very fast calculations for structures containing hundreds or thousands of atoms. The convergence and effectiveness of the cluster expansion are enhanced in two ways. First, the expansion is recast into reciprocal space, which allows for the inclusion of all important pair interactions. Second, a reciprocal-space formulation for elastic strain energy is introduced, allowing accurate predictions for both long- and short-period superlattices. We illustrate the power of the method by performing a cluster expansion that requires total-energy calculations for only 12 simple input structures, with at most eight atoms per unit cell. We then correctly predict the formation energies of relaxed long-period superlattices, low-symmetry intermixed superlattices, structures with varied compositions, substitutional impurities, and a ~ 1000 atom/cell simulation of the random alloy.

I. INTRODUCTION

Many important solid-state structures can be described as substitutional A/B systems, in which the sites of a crystal lattice are occupied by A and B atoms in different patterns. These include abrupt and intermixed superlattices, substitutional impurities and impurity aggregates, ordered $A_p B_q$ superlattices, and random $A_{1-x} B_x$ alloys. In theoretical studies of the energetics of substitutional systems it is often necessary to find ground-state configurations for a given lattice type, or to calculate finite-temperature thermodynamic averages. These applications require, in principle, sampling of the 2^N possible configurations for placing A and B atoms on N lattice sites. A unified, first-principles theoretical study of substitutional systems presents a major challenge since (i) the number of possible configurations increases exponentially with the number of lattice sites N and (ii) it may be necessary to calculate the energy of configurations with many atoms. Since the computational effort for quantum-mechanical total-energy calculations increases rapidly with the number of atoms in the unit cell, direct first-principles studies are usually limited to a small subset of the configuration space, i.e., about 10–20 structures with $\lesssim 50$ atoms out of a total of 2^N structures. These limitations make it difficult to use direct first-principles total-energy calculations to determine the ground-state configuration, the energy of the random alloy, or the temperature-composition phase diagram. Indeed, in previous studies of substitutional systems,^{1–3} the energy was parametrized empirically—an approach that has limited accuracy and only works for certain systems.

The most promising general approach to the energetics of substitutional systems is the cluster expansion (CE),^{4–8} in which the energies of the different structures are described by an Ising Hamiltonian. In the cluster

expansion, the alloy is treated as a lattice problem: the lattice sites are fixed at those of the underlying lattice (fcc, bcc, etc.) and a configuration σ is defined by specifying the occupation of each of the N lattice sites by an A atom or a B atom. (This procedure must be modified for certain compounds where the underlying lattice changes as x changes.) For each configuration, one assigns a set of “spin” variables \hat{S}_i ($i = 1, 2, \dots, N$) to each of the N sites of the lattice, with $\hat{S}_i = -1$ if site i is occupied by an A atom, and $\hat{S}_i = +1$ if it is occupied by a B atom. For a lattice with N sites, the problem of finding the energies of the 2^N possible configurations can be *exactly*⁹ mapped into a Ising Hamiltonian:

$$E(\sigma) = J_0 + \sum_i J_i \hat{S}_i(\sigma) + \sum_{j < i} J_{ij} \hat{S}_i(\sigma) \hat{S}_j(\sigma) + \sum_{k < j < i} J_{ijk} \hat{S}_i(\sigma) \hat{S}_j(\sigma) \hat{S}_k(\sigma) + \dots \quad (1)$$

for configuration σ , where the J 's are “interaction energies,” and the first summation is over all sites in the lattice, the second over all pairs of sites, the third over all triplets, and so on. The primary advantage of the cluster expansion is that the interaction energies J are the same for all configurations σ . Thus, once the J 's are known, the energy $E(\sigma)$ of any configuration can be calculated almost immediately by simply calculating the spin products and summing Eq. (1). Because the Ising representation of the energy can be calculated rapidly, and is also a linear function of the spin products, one can readily (i) apply linear programming techniques to find ground-state structures¹⁰, (ii) use statistical-mechanics techniques (Monte Carlo and cluster variation methods) to calculate phase diagrams,^{11,12} and (iii) calculate the energy of an arbitrarily complex configuration.¹³

The Hamiltonian of Eq. (1) contains 2^N interaction

energies J , which are used to describe the energies of the 2^N configurations σ . Consequently, Eq. (1) can be viewed as defining a set of linear equations, in which a $2^N \times 2^N$ matrix of spin products multiplies a 2^N vector of J 's, giving a vector of the energies of the 2^N configurations. Viewed this way, it is obvious that the J 's of Eq. (1) can be solved for exactly if the matrix of spin products is nonsingular. Actually, Sanchez, Ducastelle, and Grati⁹ have proven that the matrix is orthogonal, which guarantees that Eq. (1) is always solvable.

Were we to stop here, the cluster expansion would be completely worthless; calculating the 2^N J 's is as hard as calculating the energies of the 2^N configurations. However, intuition suggests that interactions between distant sites are less important than those between near sites, and that interactions that involve many sites are less important than those that involve fewer sites. Thus the number of J 's needed in practice may be much smaller than 2^N . If this is the case, then one can determine the J 's from the energies of a small set of configurations $\{\sigma'\}$ whose energies are calculated directly (independently of the CE, e.g., by first-principles total-energy methods or embedded atom schemes). These J 's can then be used in Eq. (1) to predict the energies of new configurations $\{\sigma''\}$. The quality of the CE is determined by comparing the energies for configurations $\{\sigma''\}$ determined by the CE with the energies determined by a direct calculation.^{8,11,13} If necessary, one can repeat this procedure by adding extra J 's until the predicted energies for $\{\sigma''\}$ are smaller than some prescribed tolerance. Two recent examples of such tests were performed for the Madelung energies on a fcc lattice (using the Ewald summation technique for the direct calculations)¹⁴ and for the energies of AlAs/GaAs on a zinc-blende lattice (where the direct calculations were done using local-density total-energy calculations).¹³ In both cases, direct calculations for a few (~ 10) simple, ordered structures defined a CE that can predict the remaining configurations with a precision comparable to that of the direct calculations. When the CE converges rapidly, the energies of the 2^N configurations are approximately linearly dependent, so that knowing a few of the energies allows us to determine the rest. Thus the advantage of the cluster expansion is that it uses the information for a small set of structures to make predictions for the energies of all other structures; by contrast, direct electronic structure calculations treat each configuration independently, and fail to take advantage of the underlying similarities among different substitutional configurations of the system.

The utility of the CE is largely determined by its rate of convergence. For systems with inherently short-ranged interactions, such as chemical interactions in size-matched alloys¹³ or magnetic exchange interactions in spin alloys,^{4,5} the CE can be applied easily—requiring ≤ 10 interactions. But when A and B have different sizes, then changing the occupancy of some sites of a given configuration will cause the atoms to relax from their original lattice positions. For example, replacing a small atom by a larger one will cause its immediate neighbors to relax outwards. The relaxation of the nearest neighbors can, in turn, cause a relaxation of their neighbors. This effect

is cumulative: if several consecutive atoms are replaced by larger atoms, then the relaxation of their neighbors will be even greater. This does not pose a formal problem for the CE because Eq. (1) can be applied to *any* quantity that is a unique property of the configurations of the system. (Different properties will, of course, have different J 's.) This includes the energy of any relaxed configurations, since this energy is a unique function of the unrelaxed configuration.^{15,16} (The relaxed configuration is the local minimum-energy configuration, which is reached by relaxing all atoms simultaneously from the starting configuration. This excludes spin flips from the relaxation process. Were spin flips allowed, all starting configurations would relax to the ground-state configuration, which is the global energy minimum. We examine only coherent structures which do not contain misfit dislocations.)

Unfortunately, cluster expansions for systems with lattice relaxation converge much more slowly than cluster expansions for unrelaxed systems. This can be seen from the contribution of the relaxations to the pair interaction energies:

$$\Delta J_{i,j} = - \sum_{k,l} \mathbf{F}(\mathbf{R}_i - \mathbf{R}_k) \cdot \Phi^{-1}(\mathbf{R}_k - \mathbf{R}_l) \cdot \mathbf{F}(\mathbf{R}_j - \mathbf{R}_l), \quad (2)$$

where $\mathbf{F}(\mathbf{R}_j - \mathbf{R}_l)$ is the force on site \mathbf{R}_l induced by the atom at site \mathbf{R}_j ("Kanzaki force") (Refs. 17 and 18) and $\Phi(\mathbf{R}_k - \mathbf{R}_l)$ is the force constant matrix. In many systems the force constants decay slowly along particular directions so the relaxations will propagate for long distances; such is the case for zinc-blende semiconductors, where the force constants decay slowly along the $\langle 011 \rangle$ bond chains. This is related to the long-range components of the force constant matrix, a phenomenon well known in phonon theory (Ref. 17 and references therein). Indeed, previous cluster expansions for relaxed fcc transition-metal alloys,¹⁶ SiGe,¹⁷ and zinc-blende semiconductors¹¹ converged much more slowly than the cluster expansions for the same system without relaxation. The effects of atomic relaxations are, however, too important to neglect. For example, relaxation lowers the miscibility-gap temperature in semiconductor alloys by several hundred degrees,¹¹ alters the relative stability of different ordered transition-metal compounds,¹⁹ and causes large (~ 1 eV) shifts in the density-of-states peaks for transition-metal alloys.²⁰

In direct calculations, the relaxed energy is calculated by minimizing the total energy of the system with respect to atomic positions, where the relaxations are required to maintain the space-group symmetry of the unrelaxed structure. The minimization requires calculations of forces and must be repeated for each configuration. In a CE that incorporates the effects of relaxation in the J 's, by contrast, the energy of any relaxed configuration is calculated simply by summing over Eq. (4); calculations of forces and relaxed geometries are not needed.

We describe an efficient, general way to incorporate relaxations into the CE. The method is based on a reciprocal-space version of Eq. (1), the concentration

wave method of Khachatryan.¹⁸ Unlike Ref. 18, we do not use the concentration wave formalism to calculate interaction energies from small amplitude waves. Instead, we fit first-principles total energies to the concentration wave equations. Also, unlike previous implementations of the concentration wave method in which the chemical interaction energies are derived from perturbations on the coherent potential approximation and relaxations are neglected,^{21–25} we determine the interaction energies from direct first-principles calculations of relaxed structures. We use the reciprocal-space representation $J(\mathbf{k})$ of the interaction energy to introduce two major improvements to the conventional CE. First, we apply a “smoothness” condition to $J(\mathbf{k})$, which corresponds to the condition that the real-space interaction energies decay with distance. With this condition, we can use a set of interactions in the CE that is much larger than the set of input structures, and the CE will naturally choose the important interactions with the smallest possible range from the set. A conventional CE, by contrast, is limited to a set of interaction energies that is no greater than the number of input structures used to fit the interactions,⁷ and therefore requires identification in advance of the important interactions. Second, we use the reciprocal-space description to identify the cause of the slow decay of the real-space interactions in size-matched systems: the strain energy of these systems leads to a singularity in $J(\mathbf{k})$ at $\mathbf{k} = \mathbf{0}$, which corresponds to an infinite set of real-space interactions. We will show that without a correct treatment of this strain term, the CE predicts the wrong energies for long-period superlattices in all directions—and the failure begins for periods $p \geq 3$. We isolate this singularity and add it as a separate term to the reciprocal-space CE. This allows us to correctly predict the formation energies of strongly relaxing structures, including the long-period superlattices.

Our CE requires the direct calculation of the formation energies of an input set of 10–20 ordered structures with small unit cells (\leq eight atoms). We demonstrate the reliability of the CE by performing direct calculations for a set of “new” structures (structures that are not members of the input set), and comparing the directly calculated energies with those predicted by the CE for these structures. We use a large set of new structures—more than 100, including long-period superlattices, superlattices with intermixed interfaces, substitutional impurities, and 1000-atom simulation of the random alloy. This set includes structures with low symmetry and large relaxations. Our CE makes accurate predictions for all of these cases. This approach offers a useful alternative to direct simulation methods for substitutional systems in that the energies of relaxed systems can be determined without knowing the relaxed geometry of each structure.

II. REAL-SPACE CLUSTER EXPANSIONS

The lattice symmetry reduces the number of interaction energies that must be determined. Since the J 's are independent of configuration, it follows that they have the symmetry of the underlying empty lattice, which is generally higher than the symmetry of any of the configura-

tions (other than pure A and pure B). For example, all lattice sites of the most common lattices (simple cubic, fcc, bcc, diamond, and hexagonal lattices) are equivalent. It follows immediately that the point interaction $J_i = J_1$ for all sites i , and the sum over single sites in Eq. (1) reduces to $NJ_1 \sum_i \hat{S}_i = NJ_1(2x - 1)$. Similarly, the interaction energies are the same for all pairs of the same type; for the common lattices, this reduces to one interaction energy for all nearest-neighbor pairs, one interaction energy for second-neighbor pairs, and so forth. In general, a set of lattice sites, called a “figure,” has the same interaction energy as any other figure that is related to it by the space-group symmetry of the underlying lattice. (Note that, as in the case of a Ge-Si alloy, the underlying lattice here is not necessarily a Bravais lattice.) We can define a correlation function $\bar{\Pi}$ for each class of symmetry-equivalent figures F as the average for each configuration of the spin products over all figures that make up F :

$$\bar{\Pi}_F(\sigma) = \frac{1}{O_F} \sum_f \hat{S}_{i_1}(\sigma) \hat{S}_{i_2}(\sigma) \dots \hat{S}_{i_m}(\sigma), \quad (3)$$

where f runs over the O_F figures in class F , and the spin indices run over the m sites of figure f . We can now rewrite Eq. (1) as

$$E_{\text{CE}}(\sigma) = N \sum_F D_F J_F \bar{\Pi}_F(\sigma), \quad (4)$$

where D_F is the number of figures of class F per site. In the remainder of this paper, we will use the term “figure” for a class of equivalent figures, as in “the nearest-neighbor pair figure.”

As mentioned, the challenge of the cluster expansion method is how to determine the interaction energies J . There are three general approaches to this problem.

The first approach is to do a purely empirical fit of the J 's to known features of the phase diagram for the alloy system^{26–28}. For example, information about the values of the J 's may be extracted from experimental critical temperatures. This approach is the simplest, but it provides little new information about the properties of the alloy. Furthermore, it was shown²⁹ that for size-mismatched systems the J 's extracted from fitting experimental critical temperatures fail to reproduce the observed mixing enthalpies.

The second approach is to determine the J 's by treating ordered structures as perturbations of the random alloy. The random alloy is treated using either the virtual crystal approximation¹⁷ or the coherent potential approximation,^{22–24} and the electronic band structure is treated with the tight-binding method^{22–24} or the Korringa-Kohn-Rostoker method.^{21,25} Methods based on these approaches include the generalized perturbation method of Ducastelle²² which was applied to many transition-metal alloys, and the linear response theory method, which was applied to the Ge-Si alloy system.¹⁷ Here, the random alloy is treated by applying virtual crystal approximation within the pseudopotential method. The interaction energies are then calculated using first-order perturbation theory, where the difference

between the Ge and Si pseudopotentials is the perturbation. This method provides accurate, first-principles results, but it is limited to alloys in which the atomic species are similar enough for low-order perturbation theory to work, and is only practical for calculating pair interaction energies.

The third approach is the direct inversion method of Connolly and Williams.^{7,8,29–33} In this method, N_σ configurations are selected for direct electronic structure calculations. The excess energy of a structure σ with composition $A_{1-x}B_x$ at volume V is defined by

$$\Delta E(\sigma, V) = E(\sigma, V) - [(1-x)E(A, V_A) + xE(B, V_B)], \quad (5)$$

where $E(A, V_A)$ and $E(B, V_B)$ are the energies of pure A and B at their equilibrium volumes V_A and V_B . The directly calculated formation enthalpy is defined by

$$E_{\text{direct}}(\sigma) = \Delta H(\sigma) = \Delta E(\sigma, V_\sigma) = \min_V \Delta E(\sigma, V), \quad (6)$$

where V_σ is the equilibrium volume of configuration σ and all structural degrees of freedom are relaxed. One also chooses N_F figures, with $N_F \leq N_\sigma$, such that the cluster expansion of Eq. (4) is converged when the sum is restricted to these N_F figures. The correlation functions and the calculated energies for these configurations are then used to fit the interaction energies of Eq. (4), by minimizing

$$\sum_{\sigma} w_{\sigma} \left(E_{\text{direct}}(\sigma) - N \sum_F D_F J_F \bar{\Pi}_F(\sigma) \right)^2 \quad (7)$$

with respect to the N_F values of J_F , where w_{σ} are weights. In this work we will choose the weights according to the formula $w_{\sigma} = 48/N_c(\sigma)$, where $N_c(\sigma)$ is the number of operations in the point group of configuration σ . (This scheme gives the highest weights to the least symmetric configurations, since these should contain more distinct environments than the high-symmetry configurations.) Equation (7) can be minimized using the singular value decomposition technique.³⁴ For the special case of $N_\sigma = N_F$ (which is the case used by Connolly and Williams,⁷) we can solve explicitly for the J 's in terms of the E 's:

$$D_F J_F = \sum_{\sigma'} [\bar{\Pi}_F(\sigma')]^{-1} E_{\text{direct}}(\sigma'). \quad (8)$$

This equation highlights the differences between the CE and the conventional interatomic potentials. In the latter, E_{direct} is written as a sum of two-body (V_{ij}), three-body (V_{ijk}), and higher potentials, so that Eq. (8) becomes

$$D_F J_F = \sum_{\sigma'} [\bar{\Pi}_F(\sigma')]^{-1} \left[\sum_{ij} V_{ij} + \sum_{ijk} V_{ijk} + \dots \right]. \quad (9)$$

Thus each J in the inversion method renormalizes in it all interatomic potentials (two-body, three-body, etc., summed over all interatomic distances), so that even the

nearest-neighbor pair interaction of the CE contains information from *all* interatomic potentials.

The advantages of the inversion approach are that it can be applied to a wide class of alloy systems, including both intermetallic and semiconductor alloys, and—when combined with *ab initio* total-energy methods—can provide accurate first-principles results. This method can also be used for cluster expansions of other calculated properties beside total energies, such as band gaps³⁵ or bond lengths.¹¹ We will use the direct inversion method in our discussion of relaxation problems.

III. RELAXATION PROBLEMS WITH THE CLUSTER EXPANSION

We will apply the CE to the GaP/InP system. Since GaP and InP have a lattice mismatch of about 7%, this will provide us with a good test of CE's in systems with large atomic relaxations. Although the underlying lattice for both GaP and InP is zinc-blende, in the CE we treat the system as a fcc lattice where each GaP unit is treated as an A "atom," and each InP unit is treated as a B atom. Within this definition, the A and B "atoms" are no longer spherically symmetric; as a result the appropriate symmetry for the GaP/InP CE is the T_d^2 space group of the zinc-blende structure, not the O_h^5 space group of the fcc structure. Since the goal of this work is to test the abilities of the CE to describe relaxation accurately, any method can be used for the direct total-energy calculations, so long as it includes realistic atomic relaxations. To this end we will calculate the energies E_{direct} using the valence force field (VFF) model of Keating,³⁶ with the force constants determined by Martin,³⁷ which allows for rapid calculation of the energies of hundreds of structures, including structures with many atoms. All of the atomic positions are fully relaxed in the VFF calculation (with the condition that the relaxations preserve the symmetry of the structure). We can then compare the CE predictions for a structure with direct VFF calculations for the same structure to assess the quality of different approaches to the CE. For future applications, the direct total-energy calculations can be performed with more accurate first-principles total-energy methods, such as the linearized augmented plane-wave method³⁸ or the pseudopotential method.³⁹

To illustrate the effects of relaxation we have used $N_\sigma = 20$ ordered structures for $A=\text{GaP}$ and $B=\text{InP}$, calculated their fully relaxed formation energies $\Delta H(\sigma)$ [Eq. (6)] with the VFF model, and obtained the interaction energies from Eq. (7). The N_σ ordered structures are all superlattices of the form $A_p B_q$, with $p, q \leq 2$ and the superlattice directions [001], [011], [111], [201], and [311]. The compositions of these structures were $x = 0, 1/4, 1/3, 1/2, 2/3, 3/4, \text{ and } 1$. The interaction energies used in CE are J_0, J_1 , the first seven pair interactions, and the first three-body and four-body interactions. Figure 1 contrasts the predictions [Eq. (4)] of this CE (dotted lines) with the results of direct calculations [Eq. (6), solid lines] for the formation energies of $(\text{GaP})_p(\text{InP})_p$ with $1 \leq p \leq 20$. The VFF results for $p = 1, 2$ (circles) were used to fit the J 's of the CE; the CE energies

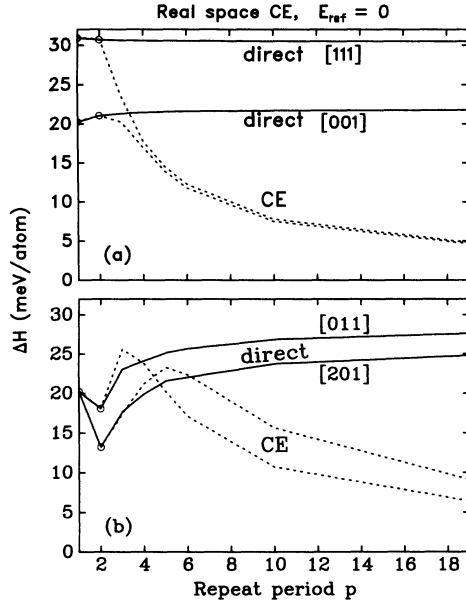


FIG. 1. Formation energies for GaP/InP superlattices as a function of repeat period p and of superlattice direction. Solid lines are results calculated with the VFF model. Dashed lines are results of a real-space cluster expansion of the VFF energies using a set of input structures with $p \leq 2$, and interaction energies J_0, J_1, J_3, J_4 , and the first seven pair interactions. The correct formation energy for long periods tends to a constant strain energy that is a function of direction, but the cluster expansion results tend to zero for all directions.

for $p \geq 3$ are pure predictions. Note that the CE begins to fail even for $p = 3$. Including structures with periods 3 and 4 in the fit delays the failure of the CE to somewhat longer periods, but direct calculations for longer-period superlattices can be very expensive. Also, including superlattices with periods 3 or higher makes the CE much worse at predicting the energies of shorter-period structures. The most disturbing feature of Fig. 1 is that it fails completely for the long-period superlattice limit. The true long-period limit for the formation energy of a coherent superlattice in the direction \mathbf{G} is the constituent strain (CS) energy⁴⁰ of the two components: $\Delta H(p \rightarrow \infty, \mathbf{G}) = \Delta E_{\text{CS}}(\mathbf{G})$. The constituent strain energy is associated with a coherent relaxation of the atoms. Since InP has a larger lattice constant than GaP, the InP region of the superlattice expands, compared to the ideal cubic lattice, while the GaP region contracts, producing a large shift of the interface position. The constituent strain energy is the combined epitaxial strain energies of the InP and GaP regions, both of which are distorted to fit a common substrate lattice constant a_{\perp} in the direction perpendicular to \mathbf{G} , but are free to relax along the \mathbf{G} direction.⁴⁰ Because the extent of the expansion and contraction is determined by the elastic constants of GaP and InP, which vary with direction, the constituent strain energy is also a function of the superlattice direction. A finite-ranged CE is completely incapable of capturing either the concerted relaxation that determines the strain energy or the directional dependence that it causes; it

predicts $\Delta H \rightarrow 0$ as $p \rightarrow \infty$.

The long-period superlattice problem is intrinsic to the CE in that any finite cluster expansion will predict that the superlattice formation energy goes to zero in the long-period limit. The reason for this failure is simple: the CE sees all A atoms that are far from the interface as if they were in a bulk A crystal, since the figures of a finite CE connect them exclusively to other A atoms. Similarly, the CE treats almost all B atoms as bulk B . As a result, the formation energy per atom in the long-period superlattice limit of the CE is zero—the formation energy of both bulk A and bulk B —and the CE completely misses the constituent strain present in coherent superlattices.

IV. ANALYSIS OF RELAXATION AND OF ITS PREVIOUS TREATMENTS

We may gain insight into how relaxations slow down the convergence of the CE and how relaxations were treated in previous approaches to the CE, by decomposing the excess energy at fixed volume of an AC/BC system. The purpose of this decomposition is to help us understand the role of relaxation in CE's. Our method of calculation, however, does not depend on this decomposition. We use the following decomposition:

$$\Delta E(\sigma, V) = \Delta E_{\text{VD}}(x, V) + \delta E_{\text{UR}}(\sigma, V) + \delta E_{\text{C}}(\sigma, V) + \delta E_{A,B}^{\text{int}}(\sigma, V) + \delta E^{\text{ext}}(\sigma, V). \quad (10)$$

The first term is the “volume deformation” (VD) energy required to change the volume of AC from V_{AC} to V , and that of BC from V_{BC} to V :

$$\Delta E_{\text{VD}}(x, V) = (1-x)[E(AC, V) - E(AC, V_{AC})] + x[E(BC, V) - E(BC, V_{BC})]. \quad (11)$$

This term can simply be pulled out of the CE, calculated directly as a function of x , and added back to the results of the CE of $\Delta E(\sigma, V) - \Delta E_{\text{VD}}$.^{8,11,17} Since ΔE_{VD} depends primarily on x and not on the individual configuration (the dependence of V on σ for a fixed x is so small that it can be ignored), it affects neither the ordering temperature nor relative energies of configurations at a fixed composition. It could, however, determine whether or not a homogeneous ordered phase will decompose into its constituents. Neglect of ΔE_{VD} (Ref. 41) can lead to the wrong sign for the formation energy and the wrong conclusions about ordering, as shown in Ref. 19. A simple way to deal with the volume dependence is to treat the J 's as functions of volume, rather than constants, and to fit $J(V)$ from $\Delta E(\sigma, V)$ [Eq. (5)] rather than from $\Delta H(\sigma)$ [Eq. (6)]; the equilibrium volume will depend on the composition if A and B have different sizes.^{7,15} An approximate version of this approach is to perform the cluster expansion on $E(\sigma) - E_{\text{ref}}(\sigma)$, where E_{ref} is a single, concentration-dependent term that represents the volume dependence.²⁹ A simple approximation for the ΔE_{VD} term is $E_{\text{ref}} = \Omega x(1-x)$, where the constant Ω may either be treated as a fitting parameter, or the result of direct calculations for the volume deformation energies of A and B .

The second term δE_{UR} is the energy difference between the unrelaxed (UR) structure (all atoms at ideal lattice sites) and ΔE_{VD} . This is often termed the “chemical” or “spin-flip” energy, and is the only term that does not vanish for size-matched systems. Classic Ising models⁴ treat only this energy.

The third term δE_C is the energy gained when the common C atoms (P for GaP/InP) are relaxed, but the A and B atoms are held in their ideal positions. In binary $A_{1-x}B_x$ systems, where there are no common C atoms, there is, of course, no δE_C . The importance of δE_C was first highlighted by EXAFS measurements on $A_{1-x}B_xC$ alloys⁴² that showed that the $A-C$ and $B-C$

bond lengths were closer to the bond lengths in pure AC and pure BC than to the average bond length of the alloy. Subsequent calculations^{30,43–45} showed that δE_C is the dominant relaxation in AC/BC semiconductor alloys.

$\delta E_{A,B}^{int}$ is the energy gained when all atoms are relaxed, but the unit cell is kept cubic. This relaxation is zero in certain high-symmetry structures, such as the A_1B_1 [001] superlattice (the $L1_0$ structure), the A_1B_3 [201] superlattice ($D0_{22}$), and the Luzonite A_1B_3 structures ($L1_2$). New EXAFS measurements on binary systems⁴⁶ reveal large cell-internal $A-B$ relaxations. Calculations by Lu and co-workers^{16,20} show that these relaxations have a significant effect on the density of states and the mixing

TABLE I. Direct VFF energies and cluster expansion (CE) predictions for $(\text{GaP})_p(\text{InP})_p$ superlattices for components of Eq. (10), in meV/atom. The last line gives the root-mean-square prediction error for each CE. For GaP/InP at $x = 1/2$, $\Delta E_{VD} = 73.84$ meV/atom.

G	p	δE_{UR}		δE_C		$\delta E_{A,B}^{int}$	
		Direct	CE	Direct	CE	Direct	CE
[001]	1	-1.438	-1.438	-50.754	-50.819	0.000	0.057
[001]	2	-0.719	-0.719	-27.205	-27.271	-23.389	-23.332
[001]	3	-0.479	-0.479	-18.184	-18.321	-32.352	-20.548
[001]	4	-0.359	-0.360	-13.639	-13.844	-36.868	-16.156
[001]	5	-0.287	-0.288	-10.911	-11.103	-39.578	-13.428
[001]	6	-0.239	-0.240	-9.093	-9.294	-41.385	-11.495
[001]	10	-0.143	-0.144	-5.456	-5.611	-44.998	-7.012
[001]	20	-0.072	-0.072	-2.728	-2.839	-47.709	-3.484
[001]	50	-0.028	-0.029	-1.091	-1.175	-49.335	-1.359
[011]	1	-1.438	-1.438	-50.754	-50.819	0.000	0.057
[011]	2	-1.078	-1.079	-43.492	-43.179	-10.445	-10.765
[011]	3	-0.719	-0.719	-27.714	-27.683	-21.406	-18.555
[011]	4	-0.539	-0.539	-21.337	-21.470	-26.700	-18.710
[011]	5	-0.431	-0.431	-17.080	-17.236	-29.961	-16.679
[011]	6	-0.359	-0.360	-14.237	-14.446	-32.245	-14.612
[011]	10	-0.215	-0.216	-8.542	-8.729	-36.727	-9.213
[011]	20	-0.107	-0.108	-4.271	-4.402	-40.093	-4.646
[011]	50	-0.043	-0.043	-1.708	-1.800	-42.112	-1.824
[111]	1	-1.078	-1.079	-39.426	-39.113	-0.799	-1.119
[111]	2	-0.539	-0.539	-20.795	-20.672	-20.059	-20.190
[111]	3	-0.359	-0.360	-13.885	-13.980	-27.179	-17.401
[111]	4	-0.269	-0.270	-10.414	-10.582	-30.754	-13.403
[111]	5	-0.215	-0.216	-8.331	-8.490	-32.899	-11.020
[111]	6	-0.179	-0.180	-6.943	-7.100	-34.329	-9.380
[111]	10	-0.107	-0.108	-4.166	-4.292	-37.189	-5.675
[111]	20	-0.054	-0.054	-2.083	-2.179	-39.334	-2.810
[111]	50	-0.021	-0.022	-0.833	-0.911	-40.621	-1.090
[201]	1	-1.438	-1.438	-50.754	-50.819	0.000	0.057
[201]	2	-1.438	-1.438	-58.659	-58.724	0.000	0.057
[201]	3	-1.198	-1.198	-46.615	-46.494	-7.907	-7.704
[201]	4	-0.898	-0.899	-35.336	-35.179	-17.163	-16.187
[201]	5	-0.719	-0.719	-28.117	-28.101	-22.770	-19.054
[201]	6	-0.599	-0.599	-23.804	-23.925	-26.694	-19.092
[201]	10	-0.359	-0.360	-14.295	-14.491	-34.575	-13.882
[201]	20	-0.179	-0.180	-7.147	-7.306	-40.582	-7.336
[201]	50	-0.072	-0.072	-2.859	-2.963	-44.182	-2.914
rms prediction error			0.001		0.150		24.002

enthalpy of binary alloys. Finally, the cell-external relaxation energy δE^{ext} is the energy gained when the unit cell vectors are allowed to relax. This term vanishes by symmetry for the Luzonite structure, and is small (~ 1 meV/atom) for the GaP/InP structures studied here.

This decomposition of the relaxation will serve as a basis for a brief review of previous treatments of relaxation within the CE. (i) In some work,^{21–25,41,47} relaxation was neglected altogether. (ii) In previous Connolly-Williams cluster expansions^{7,15,31,32} only high-symmetry short-period structures were used as input, so the important effects of $\delta E_{A,B}^{\text{int}}$ and δE^{ext} went unnoticed. (iii) Others just include the volume relaxation, either by using volume-dependent interaction energies^{7,15,30–33} or by adding an $\Omega x(1-x)$ term to the CE.²⁹ None of these techniques, however, captures the effects of δE_C and $\delta E_{A,B}^{\text{int}}$, which are *cell-internal* relaxations. (iv) A number of calculations on semiconductor alloys^{30,48} included δE_C , but neglected all or part of $\delta E_{A,B}^{\text{int}}$. (v) A recent calculation on $\text{Cu}_{1-x}\text{Au}_x$ included δE^{ext} , but neglected cell-internal relaxations.⁴⁹ Finally, (vi) calculations that incorporate all terms of Eq. (10) (Refs. 8, 11, 16, 17, 19, and 20) did not include an orientation-dependent E_{ref} , so the results are not valid for long-period superlattices.

Table I compares the values of δE_{UR} , δE_C , and $\delta E_{A,B}^{\text{int}}$ obtained from direct calculation and from a cluster expansion. The cluster expansion works perfectly well for the unrelaxed lattice— δE_{UR} is captured exactly by a sin-

gle nearest-neighbor pair interaction. δE_C is the dominant relaxation for short-period superlattices, where it leads to very large energy lowerings, but vanishes as $p \rightarrow \infty$. It too is very accurately represented by a short-ranged CE with four pair interactions. This is illustrated in Fig. 2(a), which shows direct and CE energies for $\Delta E_{\text{VD}}(x, V) + \delta E_{\text{UR}}(\sigma, V) + \delta E_C(\sigma, V)$ for superlattices as a function of p . The figure also shows that the CE captures this energy almost exactly. The long-period limit of this quantity is ΔE_{VD} for all superlattice directions. The dominant form of relaxation for medium- and long-period superlattices is $\delta E_{A,B}^{\text{int}}$ but, as shown in Fig. 2(b), this term is not properly represented by the CE, which predicts $\delta E_{A,B}^{\text{int}} = 0$ as $p \rightarrow \infty$. (Note, however, that the difference between the behavior of the C relaxation and the A - B relaxation in the long-period limit does not arise from any chemical difference between the A, B vs the C atoms, but rather from the order in which the atoms are allowed to relax.) The relaxations in the long-period superlattice can only occur if all of the atoms are allowed to move in tandem; it is therefore absent when we relax only the C atoms, but present when we relax the A and B atoms as well as the C atoms. Were we to reverse the order of relaxation, and first relax the A and B atoms, then we would have $\delta E_{A,B}^{\text{int}} = 0$ in the long-period limit, rather than δE_C .

V. RECIPROCAL-SPACE CLUSTER EXPANSION

In this section we will show that a reciprocal-space CE provides an effective way to deal with systems that have slowly converging cluster expansions. The basic idea of the reciprocal-space expansion is to replace the individual real-space interaction energies J_F , where the interaction energy of one figure has no relationship with the interaction energy of any other, with a single reciprocal-space function $J(\mathbf{k})$ on which we impose a smoothness condition, which minimizes the gradient of $J(\mathbf{k})$. Using this smoothness condition we will find a set of J 's that converges rapidly and, at the same time, correctly predicts the energies of arbitrary configurations. We will first describe the mathematical formalism of the reciprocal space expansion, and then show how the method works in practice.

A. Mathematical formalism

To recast the CE in reciprocal space, we first Fourier transform the spin products:

$$S(\mathbf{k}, \sigma) = \frac{1}{N} \sum_l^N S_l(\sigma) e^{i\mathbf{k} \cdot \mathbf{R}_l}; \quad (12)$$

the inverse transform is

$$S_l(\sigma) = \sum_{\mathbf{k}} S(\mathbf{k}, \sigma) e^{-i\mathbf{k} \cdot \mathbf{R}_l}, \quad (13)$$

where the sum over \mathbf{k} in Eq. (13) runs over the first Brillouin zone. The $S(\mathbf{k}, \sigma)$ functions have a very useful feature: for an ordered configuration σ , $S(\mathbf{k}, \sigma)$ will only be

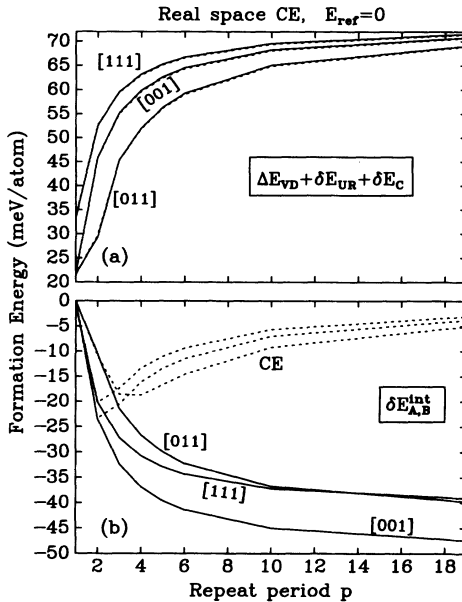


FIG. 2. (a) Formation energies for GaP/InP superlattices as a function of repeat period p when only the common P atoms are allowed to relax. (b) Energy gained when the Ga and In atoms are also allowed to relax (cell-internal AB relaxation energy). The cell basis vectors are not relaxed. Solid lines are results calculated with the VFF model. Dashed lines are results of a cluster expansion of the VFF results for a set of input structures with $p \leq 2$, and interaction energies J_0 , J_1 , J_3 , J_4 , and the first seven pair interactions.

nonzero for a finite set of points \mathbf{k} . The set of points for which $S(\mathbf{k}, \sigma)$ is nonzero is the ‘‘Lifshitz points’’ of the structure. In particular, the only \mathbf{k} points that can have $S(\mathbf{k}, \sigma) \neq 0$ are $\mathbf{k} = \mathbf{0}$ and the \mathbf{k} point that are reciprocal lattice vectors of the unit cell of σ . In the following, we

choose the coordinate system such that one of the lattice sites is at the origin, and we label that site $\mathbf{R}_0 = \mathbf{0}$. We will use the definition of $S(\mathbf{k}, \sigma)$ to transform the part of the CE energy due to the pair interactions [third term on the right-hand side of Eq. (1)]:

$$\begin{aligned}
 E_2(\sigma) &= \frac{1}{2} \sum_{l,m} J_{l,m} S_l(\sigma) S_m(\sigma) = \frac{1}{2} \sum_{l,m} \sum_{\mathbf{k}, \mathbf{k}'} J_{l,m} S^*(\mathbf{k}', \sigma) S(\mathbf{k}, \sigma) e^{i\mathbf{k}' \cdot \mathbf{R}_m} e^{-i\mathbf{k} \cdot \mathbf{R}_l} \\
 &= \frac{1}{2} \sum_{\mathbf{k}, \mathbf{k}'} \sum_{l,n} J_{l,l+n} S^*(\mathbf{k}', \sigma) S(\mathbf{k}, \sigma) e^{i\mathbf{k}' \cdot \mathbf{R}_n} e^{-i(\mathbf{k}-\mathbf{k}') \cdot \mathbf{R}_l} \\
 &= \frac{1}{2} \sum_{\mathbf{k}, \mathbf{k}'} \sum_n J_{0,n} S^*(\mathbf{k}', \sigma) S(\mathbf{k}, \sigma) e^{i\mathbf{k}' \cdot \mathbf{R}_n} \sum_l e^{-i(\mathbf{k}-\mathbf{k}') \cdot \mathbf{R}_l} \\
 &= \frac{N}{2} \sum_{\mathbf{k}, \mathbf{k}'} \sum_n J_{0,n} S^*(\mathbf{k}', \sigma) S(\mathbf{k}, \sigma) e^{i\mathbf{k}' \cdot \mathbf{R}_n} \delta_{\mathbf{k}, \mathbf{k}'} = \frac{N}{2} \sum_{\mathbf{k}} \left[\sum_n J_{0,n} e^{i\mathbf{k} \cdot \mathbf{R}_n} \right] |S(\mathbf{k}, \sigma)|^2, \tag{14}
 \end{aligned}$$

where n is defined such that $\mathbf{R}_m = \mathbf{R}_l + \mathbf{R}_n$, and the translational symmetry of the lattice was used to reduce $J_{l,l+n}$ to $J_{0,n}$. By defining

$$J(\mathbf{k}) = \frac{1}{2} \sum_n J_{0,n} e^{i\mathbf{k} \cdot \mathbf{R}_n} \tag{15}$$

we arrive at

$$E_2(\sigma) = N \sum_{\mathbf{k}} J(\mathbf{k}) |S(\mathbf{k}, \sigma)|^2. \tag{16}$$

We have replaced the sum over an infinite set of pair interactions with a sum over a few \mathbf{k} points. While three-body and higher figures could also be described by a reciprocal-space expansion, the formulas are too complicated for practical use. Instead three-body and four-body figures will be added as explicit real-space figures:

$$E_{\text{CE}}(\sigma) = N \sum_F' D_F J_F \bar{\Pi}_F(\sigma) + N \sum_{\mathbf{k}} J(\mathbf{k}) |S(\mathbf{k}, \sigma)|^2, \tag{17}$$

where the primed sum runs over the set of nonpair figures included in the expansion.

The functions $J(\mathbf{k})$ and $S(\mathbf{k}, \sigma)$ obey some simple sum rules:

$$\sum_{\mathbf{k}} J(\mathbf{k}) = 0, \quad \sum_{\mathbf{k}} |J(\mathbf{k})|^2 = \frac{N}{4} \sum_l J_{0,l}^2 \tag{18}$$

and

$$\sum_{\mathbf{k}} S(\mathbf{k}, \sigma) = \pm 1, \quad \sum_{\mathbf{k}} |S(\mathbf{k}, \sigma)|^2 = 1. \tag{19}$$

The values of $S(\mathbf{k}, \sigma)$ have a nonunique phase factor that depends on the choice of origin for the unit cell. Since the pair energies depend only on the magnitude of S , they are uniquely determined. Also, if the conjugate configuration $\bar{\sigma}$ of configuration σ is formed by reversing the identity of

all of the A and B atoms, then we have $S_l(\bar{\sigma}) = -S_l(\sigma)$ and $S(\mathbf{k}, \bar{\sigma}) = -S(\mathbf{k}, \sigma)$. Thus the pair energy will be the same for both σ and $\bar{\sigma}$. This is actually a special case of the general rule that for a figure F with an even number of sites $\bar{\Pi}_F(\bar{\sigma}) = \bar{\Pi}_F(\sigma)$, while for a figure with an odd number of sites $\bar{\Pi}_F(\bar{\sigma}) = -\bar{\Pi}_F(\sigma)$. As a consequence of this, if we want to describe a system in which we allow the composition x of $A_{1-x}B_x$ to change, we must include odd figures in the expansion. For if we try to use a CE with only even figures, we will find the same energy for a configuration σ with composition x as we will find for $\bar{\sigma}$, which has composition $1-x$.

B. Determining $J(\mathbf{k})$

The calculation of $S(\mathbf{k}, \sigma)$ can be done very quickly and simply, as can the sum of Eq. (17). To calculate $J(\mathbf{k})$ we will again follow the procedure of calculating the total energy directly for a small set s of input structures $\{\sigma : \sigma \in s\}$, and use the results to fit the function $J(\mathbf{k})$, just as in the Eq. (7) for the standard real-space CE.

Practicality requires that we use a small set of input structures $\{\sigma'\}$, and that each structure have ≤ 10 atoms. In Table II, we present $|S(\mathbf{k}, \sigma)|^2$ for a set of 27 ordered structures from which we will choose all of the input structures that are used in this work. The largest of these structures contains eight atoms for a zinc-blende lattice, or four for a fcc lattice. Thus each of these structures is small enough to allow accurate, first-principles calculations as a basis for future CE's.

For practical applications, we will write $J(\mathbf{k})$ as a summation over a finite set of plane waves:

$$J(\mathbf{k}) = \frac{1}{2} \sum_{R_l \leq R_M} J_{0,l} e^{i\mathbf{k} \cdot \mathbf{R}_l} = \sum_I^{N_P} D_I J_I H_I(\mathbf{k}). \tag{20}$$

Here I runs over classes of pairs $(0, l)$ that are equivalent by the symmetry of the lattice (all of which have the same $J_{0,l} \equiv J_I$), e.g., the nearest-neighbor pair fig-

TABLE II. $|S(\mathbf{k}, \sigma)|^2$ for 27 ordered structures σ . All of these structures, except pure GaP and InP (A and B) and the two Luzonite structures (L1 and L3), are $(\text{GaP})_p(\text{InP})_q$ superlattices along direction \mathbf{G} . For $p \neq q$ structures the symbol of conjugate structure, which is a $(\text{GaP})_q(\text{InP})_p$ superlattice, is listed beneath. The values of $|S(\mathbf{k}, \sigma)|^2$ are the same for a structure and its conjugate. All \mathbf{k} points are in units of $2\pi/a$.

\mathbf{G}	[111]				[001]				[011]			[201]		[311]		—	
	p, q	1,1	1,2	1,3	2,2	1,1	1,2	1,3	2,2	1,2	1,3	2,2	1,3	2,2	1,3		2,2
\mathbf{k}	A	CP	$\alpha 1$	V1	V2	CA	$\beta 1$	Z1	Z2	$\gamma 1$	Y1	Y2	F1	CH	W1	W2	L1
	B		$\alpha 2$	V3			$\beta 2$	Z3		$\gamma 2$	Y3		F3		W3		L3
[000]	1		1/9	1/4			1/9	1/4		1/9	1/4		1/4		1/4		1/4
$\frac{1}{4}[111]$				1/2	1												
$\frac{1}{3}[111]$			8/9														
$\frac{1}{2}[111]$		1		1/4												1/4	
$\frac{1}{2}[001]$								1/2	1								
$\frac{2}{3}[001]$							8/9										
[001]						1		1/4			1/4		1/4				3/4
$\frac{1}{2}[011]$										1/2	1						
$\frac{2}{3}[011]$									8/9								
$\frac{1}{2}[201]$												1/2	1				
$\frac{1}{4}[311]$															1/2	1	

ure, and the sum runs over the first N_P inequivalent pair figures. D_I is the number of equivalent pairs per lattice site. (Since each pair is shared by two sites, there are $2D_I$ pairs connected to each site.) The function H_I is a symmetrized plane wave:

$$H_I(\mathbf{k}) = \frac{1}{2D_I} \sum_I e^{i\mathbf{k} \cdot \mathbf{R}_I}, \quad (21)$$

where the sum is over the $2D_I$ pairs in class I that connect to the site $\mathbf{R}_0 = \mathbf{0}$. By combining Eqs. (4), (16), and (20), the pair energy is

$$\begin{aligned} E_2(\sigma) &= N \sum_I D_I J_I \bar{\Pi}_I(\sigma) \\ &= N \sum_{\mathbf{k}} J(\mathbf{k}) |S(\mathbf{k}, \sigma)|^2 \\ &= N \sum_I D_I J_I \sum_{\mathbf{k}} H_I(\mathbf{k}) |S(\mathbf{k}, \sigma)|^2, \end{aligned} \quad (22)$$

which implies that

$$\bar{\Pi}_I(\sigma) = \sum_{\mathbf{k}} H_I(\mathbf{k}) |S(\mathbf{k}, \sigma)|^2. \quad (23)$$

We now have an exact equivalence between a real-space expansion using N_P pair figures and a reciprocal-space expansion. By using Eqs. (20) and (23), we can easily convert from the reciprocal-space form to the real-space form and back.

Since the reciprocal-space expansion up to this point is equivalent to a real-space expansion, the two forms share the same problems. In particular, the total number of

figures included in Eq. (4) or Eq. (17) must be less than the number of structures in the set s , whose energies are used to fit J_F and $J(\mathbf{k})$. To overcome this problem, we require that $J(\mathbf{k})$ be a smooth function of \mathbf{k} . To this end we define a “smoothness value” M as

$$M = \frac{1}{\alpha} \sum_{\mathbf{k}} J(\mathbf{k}) [-\nabla_{\mathbf{k}}^2]^{1/2} J(\mathbf{k}) = \frac{N}{2\alpha} \sum_I R_I^\lambda D_I J_I^2, \quad (24)$$

where the exponent λ is a free parameter, and α is a normalization constant:

$$\alpha = \frac{N}{2} \sum_I R_I^\lambda D_I. \quad (25)$$

The smoothness condition is therefore equivalent to requiring that the pair interactions fall off rapidly for large distances. Our use of this smoothness condition will be tested when we examine the quality of predictions made using the function $J(\mathbf{k})$.

Our new fitting procedure will be to minimize

$$\sum_{\sigma \in s} w_\sigma |E_{\text{direct}}(\sigma) - E_{\text{CE}}(\sigma)|^2 + tM \quad (26)$$

by varying $\{J_F\}$ (for the nonpair figures included in the expansion) and $\{J_I\}$ (for the pair figures). Here $E_{\text{direct}}(\sigma)$ is the directly calculated energy [Eq. (6)], $E_{\text{CE}}(\sigma)$ is defined in Eq. (17), and t is a scaling factor. The scaling factor is a matter of choice, but we have found in tests that any value in the range $1 \leq t \leq 100$ produces almost identical results. Similarly, the CE shows only a slight dependence on λ in the range $4 \leq \lambda \leq 10$. Un-

less otherwise indicated, we will use $t = 1$. Note that using $t = 0$ completely eliminates the smoothness condition, and results in a plain real-space fit of Eq. (7). If we fit with a large number of figures and $t = 0$, the fitting procedure has no way of knowing which interactions are short-ranged and which are long-ranged. As a result, the long-ranged interactions will be as strong as the short-ranged interactions, which is unphysical. The chief advantage of the reciprocal-space method is that it lets the fitting procedure choose which pairs are important. Because of the smoothness criterion, any pair figure that is not strictly necessary for a good fit will have an interaction energy of zero. Also, the smoothness criterion naturally favors short-ranged over long-ranged interactions, which is physically sensible.

C. Tests of reciprocal-space cluster expansion

We are now ready to apply the reciprocal-space CE. As before, we will use the VFF model to calculate the energies $E_{\text{direct}}(\sigma)$ of different structures for the GaP/InP system. To examine the convergence of the CE we will use four different sets, $s_0 \subset s_1 \subset s_2 \subset s_3$, of input structures for the calculations, all of which are taken from the structures listed in Table II, which also defines the symbol used for each structure. These sets are

$$\begin{aligned} s_0 &= \{A, B, CA, L1, L3\} && (5 \text{ elements}), \\ s_1 &= s_0 \cup \{\text{CH}, \text{CP}, \text{Z2}\} && (8 \text{ elements}), \\ s_2 &= s_1 \cup \{\text{V2}, \text{Y2}, \text{W1}, \text{W3}\} && (12 \text{ elements}), \\ s_3 &= \text{all structures in Table II} && (27 \text{ elements}). \end{aligned}$$

The set s_0 is the standard Connolly-Williams set,⁷ while the set s_1 was previously used in real-space fits for many semiconductor alloys.¹¹ Set s_3 was previously used in a real-space CE of semiconductor band gaps.³⁵

To test the reciprocal-space versus real-space CE, we will first minimize Eq. (26) to determine the interaction energies, using each of sets s_0 , s_1 , s_2 , and s_3 . For each fit, we then predict the total energies of a large set of new structures, none of which are used in the fit. The predictions are performed for four types of structures: (i) long-period superlattices: $(\text{GaP})_p(\text{InP})_p$ superlattices with $3 \leq p \leq 6$ and $p = 10$ (20 structures); (ii) intermixed superlattices: superlattices with $p = 1, 2$ in

which some of the atoms on each side of the interface have been swapped—thereby lowering the symmetry (24 structures); (iii) $x \neq 1/2$ structures: structures in which $x \neq 1/2$, consisting of $(\text{GaP})_p(\text{InP})_q$ superlattices, with $p+q = 5$, $(\text{GaP})_1(\text{InP})_6$ and $(\text{GaP})_6(\text{InP})_1$ superlattices, and GaP (InP) supercells with 8, 16, 32, and 64 atoms, containing a single In_{Ga} (or Ga_{In}) substitutional impurity (43 structures); and (iv) large supercell simulations of random alloys: the energy of a random GaP/InP alloy is determined by averaging over different configurations of a fully relaxed 1000-atom supercell. For each of the new structures in (i)–(iv), we independently calculate the VFF formation energy and compare it with the CE prediction. The calculated formation energies for sets (i)–(iii) cover a wide range: $17.7 \rightarrow 30.6$, $14.9 \rightarrow 32.2$, and $2.2 \rightarrow 31.0$ meV/atom, respectively.

We perform the CE in three different ways, shown in panels (a)–(c) of Fig. 3. In all cases, we use the following real-space interactions in the first term of Eq. (17): J_0 , the empty figure (i.e., a constant term that is independent of σ); J_1 , a single-site term; J_3 , the nearest-neighbor three-body interaction; and J_4 , the nearest-neighbor tetrahedron interaction. Our first calculation [Fig. 3(a)] is a simple real-space CE using the first 1 through 7 pair figures, where the number of pair figures is adjusted to assure that $N_\sigma \geq N_F$. In our second calculation [Fig. 3(b)], we repeat the same real-space expansion, but expand $E - E_{\text{ref}}$, in place of E . We use the volume-deformation energy $\Omega x(1-x)$ for E_{ref} . The value of Ω is treated as a fitting parameter, and we find $\Omega = 147.1$ meV/atom, using input set s_2 . Finally [Fig. 3(c)], we repeat the latter CE, but this time using the reciprocal-space formalism, i.e., we set $t = 1$ instead of $t = 0$ in Eq. (26), which allows us to include the first 20 pair interactions. The fitted value of Ω is 129.5 meV/atom, using s_2 .

In Figs. 3(a)–3(c), we present the root-mean-square (rms) prediction error of the CE's for each of the three sets of new structures. Note that the interaction energies were fitted without any knowledge of the energies of these new structures. The predictions for the formation energy of the random alloy, using input set s_2 , are 19.90, 20.95, and 20.77 meV/atom for the three fitting procedures [Figs. 3(a)–3(c)]. Bernard⁵⁰ has calculated the VFF energy of the random alloy by averaging over many ran-

TABLE III. Root-mean-square (rms) and maximum (max) prediction errors for different cluster expansions. Errors are reported separately for long-period ($p \geq 3$) superlattices, intermixed short-period ($p < 3$) superlattices, and for structures with composition $x \neq 1/2$. The input set s_2 was used for each CE. Real-space figures J_0 , J_1 , J_3 , and J_4 were included in each CE. Lines (a), (b), (c), and (d) refer to the CE's described in panels (a), (b), (c), and (d), respectively, of Fig. 3. All energies are in meV/atom.

	Cluster expansion		Long-period SL's		Intermixed SL's		$x \neq 1/2$ structures	
	Space	E_{ref}	rms	max	rms	max	rms	max
(a)	Real	0	10.24	21.93	1.09	2.95	2.14	5.44
(b)	Real	$\Omega x(1-x)$	6.51	13.36	1.03	3.05	1.77	4.40
(c)	Reciprocal	$\Omega x(1-x)$	3.94	8.78	0.74	1.80	1.29	2.67
(d)	Reciprocal	ΔE_{CS}	1.08	2.33	0.70	1.42	0.82	2.22

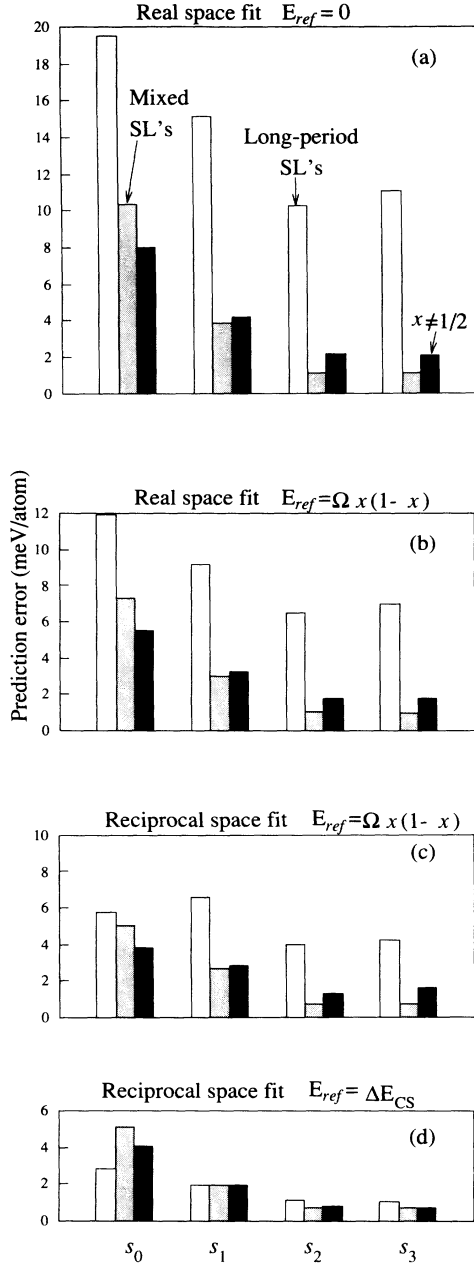


FIG. 3. Prediction errors for different CE's, in meV/atom. The CE is applied to $E - E_{ref}$ for four different fitting procedures: (a) Real-space fit with $E_{ref} = 0$ and $N_P \leq 7$. N_P is adjusted such that the number of figures is always less than or equal to the number of input structures. (b) Real-space fit with $E_{ref} = \Omega x(1-x)$ where Ω is treated as a fitting parameter and $N_P \leq 7$. (c) Reciprocal-space fit with $E_{ref} = \Omega x(1-x)$ and $N_P = 20$. (d) Reciprocal-space fit with $E_{ref} = \Delta E_{CS}$ and $N_P = 20$. Root-mean-square prediction errors (root-mean-square average of $E_{direct} - E_{CE}$) are shown separately for superlattices with $p > 3$ (open rectangles), superlattices with $p = 1, 2$ and atoms swapped across the interface (shaded rectangles), and structures with $x \neq 1/2$ (solid rectangles). Each CE is repeated using the input sets s_0, s_1, s_2 , and s_3 (defined in Sec. V C). Real-space fits have the scaling parameter $t = 0$, while reciprocal-space fits have $t = 1$ [Eq. (26)].

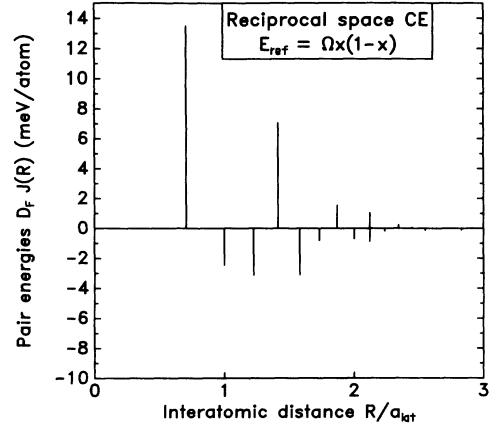


FIG. 4. Real-space pair interaction energies from the reciprocal-space fit (c) using input set s_2 and $E_{ref} = \Omega x(1-x)$.

domly generated configurations of $\text{Ga}_{0.5}\text{In}_{0.5}\text{P}$ in a 1000-atom supercell, with all atomic positions relaxed. The directly calculated formation energy for the random alloy is 20.45 meV/atom. Hence, both the real-space [3(b)] and the reciprocal-space methods [3(c)] with $E_{ref} = \Omega x(1-x)$ predict well the energy of the random alloy. As discussed above, all three CE's [3(a)–3(c)] fail to predict the energies of the longer-period superlattices. We will return to this issue in the next section.

For the intermixed structures, we see that using set s_2 of 12 input structures is adequate for making accurate predictions for all three methods. We also see that using $E_{ref} = \Omega x(1-x)$ works better than using $E_{ref} = 0$, and that the reciprocal-space expansion works better than the real-space expansion. Another indication of the superiority of the reciprocal-space expansion is the maximum error made in the CE predictions—which is a measure of how well CE predictions can be trusted. (A CE that predicts the energy 95% of structures exactly, but has a large prediction error for the remaining 5%, will have a small rms prediction error, but is not worth much because we can never be sure whether the prediction for a new structure belongs to the 95% or the 5%.) Table III

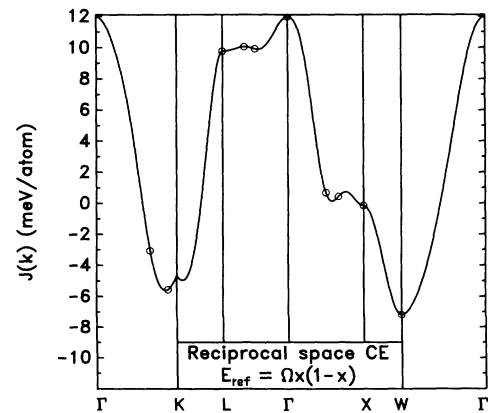


FIG. 5. $J(\mathbf{k})$ along the principal directions in the Brillouin zone for the same CE described in Fig. 4. Circles are placed on values of \mathbf{k} for which $S(\mathbf{k}, \sigma) \neq 0$ for one or more structures in the input set s_2 .

shows both the rms and the maximum prediction error of the three fitting procedures using the input set s_2 . The reciprocal-space fit [Fig. 3(c)], having much smaller maximum errors, is clearly superior to the real-space fit. In Figs. 4 and 5, we show the pair interaction energies (transformed into real space) and $J(\mathbf{k})$ of the CE for the reciprocal space fit [Fig. 3(c)] using the input set s_2 and $E_{\text{ref}} = \Omega x(1-x)$.

VI. LONG-PERIOD SUPERLATTICES

A. The long-period superlattice problem and singular $J(\mathbf{k})$

As shown in Figs. 1 and 3, the CE fails to predict the energies of lattice-mismatched superlattices—even for periods as short as $p = 3$. We explained in Sec. III that the cause of this problem is the long-range coherent relaxation of the atoms that occurs to relieve that lattice-mismatch strain. We will now demonstrate that the superlattice problem is caused by a singularity in $J(\mathbf{k})$ at $\mathbf{k} = \mathbf{0}$, so that no finite real-space or continuous reciprocal-space expansion will predict the correct limit. In the next subsection, we will show how this problem can be solved.

For the $A_p B_p$ superlattice in direction \mathbf{G} , the only \mathbf{k} points for which $S(\mathbf{k}, \sigma) \neq 0$ are those that satisfy

$$\mathbf{k} = \frac{2\pi n}{2pd_{\hat{\mathbf{G}}}} \hat{\mathbf{G}}, \quad (27)$$

where $d_{\hat{\mathbf{G}}}$ is the distance between two adjacent layers in the superlattice direction, and n is any odd integer. Placing the B atoms in the first p layers and the A atoms in the next p layers, we have

$$\begin{aligned} S(\mathbf{k}, \sigma) &= \frac{1}{2p} \sum_{l=1}^p e^{\frac{2\pi i l n}{2p}} - e^{-\frac{2\pi i l n}{2p}} (-1)^n \\ &= \frac{1}{p} \sum_{l=1}^p \exp\left(\frac{i\pi l n}{p}\right) \\ &= \frac{1}{p} \frac{\sin\left(\frac{\pi n}{2}\right) \exp\left(i\pi n \frac{p+1}{2p}\right)}{\sin\left(\frac{\pi n}{2p}\right)}. \end{aligned} \quad (28)$$

We then have

$$\lim_{p \rightarrow \infty} |S(\mathbf{k}, \sigma)|^2 = \lim_{p \rightarrow \infty} \frac{1}{p^2} \frac{1}{\sin^2\left(\frac{\pi n}{2p}\right)} = \frac{4}{\pi^2 n^2}. \quad (29)$$

Thus for the long-period superlattice, the dominant contribution to the pair energy $N \sum_{\mathbf{k}} J(\mathbf{k}) |S(\mathbf{k}, \sigma)|^2$ comes from the \mathbf{k} points with $n = \pm 1$, which contain $8/\pi^2 \cong 81\%$ of the weight of $|S(\mathbf{k}, \sigma)|^2$. In fact,

$$\lim_{p \rightarrow \infty} \sum_{\mathbf{k}} J(\mathbf{k}) |S(\mathbf{k}, \sigma)|^2 = \lim_{\mathbf{k} \rightarrow \mathbf{0}} J(\mathbf{k}). \quad (30)$$

Therefore, in the long-period limit of the CE, the superlattice energy goes to $J(\mathbf{k} = \mathbf{0})$, for all superlattice directions. But, as can be seen from Fig. 1, the correct, coherent long-period superlattice limit is different in different

directions. Thus the true $J(\mathbf{k})$ function must approach different limits at the origin along different directions. *This means that $J(\mathbf{k})$ is singular at the origin—which corresponds to an infinite real-space CE.*

B. Dealing with the singularity

We will show how it is possible to get the correct long-period superlattice limit using a cluster expansion. The basic idea is to write the reciprocal-space interaction energies as

$$J(\mathbf{k}) = J_{\text{CS}}(\mathbf{k}) + J_{\text{SR}}(\mathbf{k}), \quad (31)$$

where the first term on the right-hand side is singular at $\mathbf{k} = \mathbf{0}$ and contains the correct long-period superlattice limit, i.e., the constituent-strain energy. The continuous part J_{SR} describes the short-ranged (SR) interactions that are ignored by J_{CS} . We will subtract the constituent-strain energy from E_{direct} , and determine J_{SR} by fitting the remainder:

$$\begin{aligned} E_{\text{direct}}(\sigma) - N \sum_{\mathbf{k}} J_{\text{CS}}(\mathbf{k}) |S(\mathbf{k}, \sigma)|^2 \\ = N \sum_{\mathbf{k}} J_{\text{SR}}(\mathbf{k}) |S(\mathbf{k}, \sigma)|^2 + N \sum_F D_F J_F \bar{\Pi}_F(\sigma). \end{aligned} \quad (32)$$

The division of these parts is somewhat arbitrary; the essential feature is that the J_{CS} contain the singularity at the origin, leaving a smooth function J_{SR} , that can be fitted using the techniques of the preceding section. Since $J_{\text{CS}}(\mathbf{k})$ is singular at $\mathbf{k} = \mathbf{0}$, the corresponding real-space pair expansion has an infinite number of nonzero pair interactions. This property is to be expected, since we have shown that the constituent-strain energy cannot be represented by a finite CE.

The remainder of this section is organized as follows. First, we will explain why it is necessary to represent the constituent-strain energy by a reciprocal-space expansion. Next we give the basic form of the function $J_{\text{CS}}(\mathbf{k})$ in terms of ΔE_{CS} . We will then discuss the form of the constituent-strain expansion for short-period structures, and its properties as a function of x . We will also present a formula for ΔE_{CS} derived from elastic theory, and describe how this formula can be used to provide a practical implementation of J_{CS} . The section ends with a synopsis of the working equations and a step-by-step guide of how to use this method.

An accurate CE can be constructed by expanding $E_{\text{direct}} - E_{\text{ref}}$, and using the long-period superlattice energy for E_{ref} . The constituent-strain energy $\Delta E_{\text{CS}}(\mathbf{G})$ is defined as the long-period superlattice energy limit in the direction \mathbf{G} , which is the formation energy of pure A and pure B , each constrained to the equilibrium substrate lattice constant of the long-period superlattice limit. This would automatically include the directional dependence of the superlattice energies, but still allow a finite CE. Using $E_{\text{ref}} = \Delta E_{\text{CS}}(\mathbf{G})$ is not as easy as it looks, because

ΔE_{CS} is only well defined for long-period superlattices. In particular, the value of \mathbf{G} in $\Delta E_{CS}(\mathbf{G})$ for nonsuperlattice structures is undefined. For certain short-period superlattices, \mathbf{G} is not well defined either. For example, the monolayer superlattices in the [001], [011], and [201] directions are all identical. For this structure, which direction do we use to evaluate $\Delta E_{CS}(\mathbf{G})$?

We solve this problem by performing a reciprocal-space cluster expansion of $\Delta E_{CS}(\mathbf{G})$. We write

$$\Delta E_{CS}(\sigma) = N \sum_{\mathbf{k}} J_{CS}(\mathbf{k}) |S(\mathbf{k}, \sigma)|^2. \quad (33)$$

Since the constituent-strain energy is defined as the $p \rightarrow \infty$ limit of the superlattice energy, it must be independent of p . This condition is met if J_{CS} depends only on the direction of \mathbf{k} , not its magnitude. We therefore set

$$J_{CS}(\mathbf{k}) = J_{CS}(\hat{\mathbf{k}}) = \Delta E_{CS}(\hat{\mathbf{k}}) \text{ for } \mathbf{k} \neq \mathbf{0}, \quad (34)$$

$$J_{CS}(\mathbf{0}) = 0.$$

This form is the one used by Khachatryan.¹⁸ For an $A_p B_p$ superlattice in direction \mathbf{G} , the \mathbf{k} points for which $S(\mathbf{k}, \sigma) \neq 0$ all lie along the $\hat{\mathbf{G}}$ direction [Eq. (27)]. Using the sum rule $\sum_{\mathbf{k}} |S(\mathbf{k}, \sigma)|^2 = 1$, we have

$$\begin{aligned} \sum_{\mathbf{k}} J_{CS}(\hat{\mathbf{k}}) |S(\mathbf{k}, \sigma)|^2 &= J_{CS}(\hat{\mathbf{G}}) \sum_{\mathbf{k}} |S(\mathbf{k}, \sigma)|^2 \\ &= J_{CS}(\hat{\mathbf{G}}) = \Delta E_{CS}(\hat{\mathbf{G}}), \end{aligned} \quad (35)$$

which shows that Eq. (34) produces the correct constituent-strain energy for the superlattices.

For some short-period superlattices the \mathbf{k} points for which $S(\mathbf{k}, \sigma) \neq 0$ will fall outside the first Brillouin zone. Since J_{CS} must have the full translational symmetry of the reciprocal lattice, any \mathbf{k} point outside the first Brillouin zone must be translated to a \mathbf{k} point interior to the zone by a reciprocal lattice vector. Once the \mathbf{k} point is translated to the interior of the zone, it may lie in a direction other than $\hat{\mathbf{G}}$. Thus the constituent-strain energy is different for some short-period superlattices than for long-period superlattices along the same direction. This will not affect the strain energy of the long-period superlattices because the weight of the \mathbf{k} points that fall outside the zone goes to zero as p increases. It is precisely this feature of the constituent-strain expansion that resolves the ambiguity described above for the monolayer superlattices. As mentioned, the monolayer superlattices in the [001] and [011] directions are actually the same structure. If we treat this structure as a superlattice in the [011] direction, we will find that $S(\mathbf{k}, \sigma) = 1$ for $\mathbf{k} = [011]$. (All \mathbf{k} points are in units of $2\pi/a$.) Since this point lies outside the zone, we must translate it by the reciprocal-lattice vector $[\bar{1}\bar{1}\bar{1}]$ to the point $[00\bar{1}]$, which is equivalent to [001] by the rotational symmetry of the fcc lattice. Similarly, if we view the structure as a [201] superlattice, we must translate $\mathbf{k} = [201]$ to $\mathbf{k} = [001]$ by the reciprocal lattice vector $[\bar{2}00]$. Thus, no matter how we choose to view the structure, the reciprocal-space expansion automatically gives $\Delta E_{CS}([001])$ for the constituent-strain energy.

Equations (33) and (34) define a constituent-strain energy that gives the correct limit for the long-period superlattices and is well defined for nonsuperlattice structures and short-period superlattices. The only remaining ambiguity is for points on the Brillouin zone boundary, where points that lie along different directions may be related to one another by reciprocal lattice vectors. For such cases, one must either arbitrarily choose the value of J_{CS} of one of these directions, or else take the average value of J_{CS} for all equivalent zone boundary points. We use the second of these two approaches. This situation rarely arises in practice, however, because the only zone boundary points that occur for common structures are high-symmetry points such as [001] or [111], which can only be translated to zone boundary points in symmetry-equivalent directions. As a result the two methods give identical results in almost all cases.

We can view J_{CS} as the pair contribution to the full cluster expansion of ΔE_{CS} , which can also contain three-site, four-site, and higher interactions. From this viewpoint, J_{CS} has exactly the correct x dependence. For a superlattice in the $\hat{\mathbf{G}}$ direction with $x \neq 1/2$ we have

$$\begin{aligned} 1 &= |S(\mathbf{0}, \sigma)|^2 + \sum_{\mathbf{k} \neq \mathbf{0}} |S(\mathbf{k}, \sigma)|^2 \\ &= (2x - 1)^2 + \sum_{\mathbf{k} \neq \mathbf{0}} |S(\mathbf{k}, \sigma)|^2, \end{aligned} \quad (36)$$

$$\sum_{\mathbf{k} \neq \mathbf{0}} |S(\mathbf{k}, \sigma)|^2 = 1 - (2x - 1)^2 = 4x(1 - x), \quad (37)$$

and therefore

$$\sum_{\mathbf{k} \neq \mathbf{0}} |S(\mathbf{k}, \sigma)|^2 J_{CS}(\hat{\mathbf{G}}) = 4x(1 - x) J_{CS}(\hat{\mathbf{G}}). \quad (38)$$

Since $\Delta E_{CS}(\sigma) = 0$ for $x = 0$ or 1 , an expansion of $\Delta E_{CS}(\sigma) \equiv \Delta E_{CS}(\hat{\mathbf{G}}, x)$ in powers of x must have the form

$$\begin{aligned} \Delta E_{CS}(\hat{\mathbf{G}}, x) &= 4x(1 - x)C_2(\hat{\mathbf{G}}) \\ &\quad + 4(2x - 1)x(1 - x)C_3(\hat{\mathbf{G}}) + \dots \end{aligned} \quad (39)$$

Thus, if we choose $J_{CS}(\hat{\mathbf{G}})$ independent of x , we can identify it with the first coefficient $C_2(\hat{\mathbf{G}})$ of the x expansion of ΔE_{CS} . The higher powers of x correspond to higher-order figures in the expansion. Shortly, we will show that by choosing an x -dependent form for J_{CS} , we can include all orders of the x expansion with pair figures alone.

C. Formula for ΔE_{CS}

It remains to find a practical implementation of $\Delta E_{CS}(\hat{\mathbf{G}})$ for any direction. To do this we will use harmonic continuum elasticity theory,^{51,52} which is appropriate for the long-period limit. To begin, picture two large slabs of A and B . Initially both slabs are at their respective equilibrium volumes, and the formation energy of each slab is zero. We now deform each slab to a common substrate lattice constant in the direction per-

pendicular to the vector \hat{k} , while allowing each material to relax along the \hat{k} direction. This deformation process will require an elastic energy

$$\Delta E_{CS}(\hat{k}, x, a_{\perp}) \equiv (1-x)\Delta E_A^{\text{epi}}(\hat{k}, a_{\perp}) + x\Delta E_B^{\text{epi}}(\hat{k}, a_{\perp}), \quad (40)$$

i.e., the average energy to grow A and B epitaxially on substrate lattice constant a_{\perp} in the plane perpendicular to \hat{k} . For each direction \hat{k} , some value a_{\perp}^{eq} of the substrate lattice constant minimizes this elastic energy. The value of a_{\perp}^{eq} will depend on \hat{k} . The equilibrium-strain energy $\Delta E_{CS}^{\text{eq}}(\hat{k}, x)$ is the elastic energy for deforming the two slabs to the common substrate lattice constant a_{\perp}^{eq} :

$$\Delta E_{CS}^{\text{eq}}(\hat{k}, x) \equiv \Delta E_{CS}(\hat{k}, x, a_{\perp}^{\text{eq}}). \quad (41)$$

The preceding discussion is exact for high-symmetry directions like [001] and [111]. But for low-symmetry directions, such as [201], the substrate lattice constant is different for two different directions in the substrate plane. This can further lower $\Delta E_{CS}^{\text{eq}}(\hat{k}, x)$. We have examined the additional energy lowering for the GaP/InP system by comparing $\Delta E_{CS}^{\text{eq}}(\hat{k}, x)$ calculated within the

VFF model by the procedure used above, with the long-period limit of a series of fully relaxed $(\text{GaP})_p(\text{InP})_p$ superlattices. We find that this energy lowering is small (< 1 meV). We will ignore this extra relaxation in this work, recognizing that for certain directions we will overestimate the superlattice formation energy by a small amount.

Within this approximation, we derive in the Appendix the form of $\Delta E_{CS}^{\text{eq}}$ from continuum elasticity theory:

$$\begin{aligned} \frac{1}{\Delta E_{CS}^{\text{eq}}(\hat{k}, x)} &= \frac{1}{(1-x)\Delta E_A^{\text{epi}}(\hat{k}, a_B)} + \frac{1}{x\Delta E_B^{\text{epi}}(\hat{k}, a_A)} \\ &= \frac{1}{(1-x)q_A(\hat{k})\Delta E_A(a_B)} \\ &\quad + \frac{1}{xq_B(\hat{k})\Delta E_B(a_A)}, \end{aligned} \quad (42)$$

where $\Delta E_A(a_B) = E_A(a_B) - E_A(a_A)$, $\Delta E_B(a_A) = E_B(a_A) - E_B(a_B)$, and $E_A(a)$ and $E_B(a)$ are the energies of bulk cubic A and B at the lattice constant a . All of the directional dependence is included in the “strain-relaxation factor” $q_A(\hat{k})$ (Refs. 16, 51 and 52) defined by

$$\Delta E_A^{\text{epi}}(\hat{k}, a) = q_A(\hat{k})\Delta E_A(a), \quad (43)$$

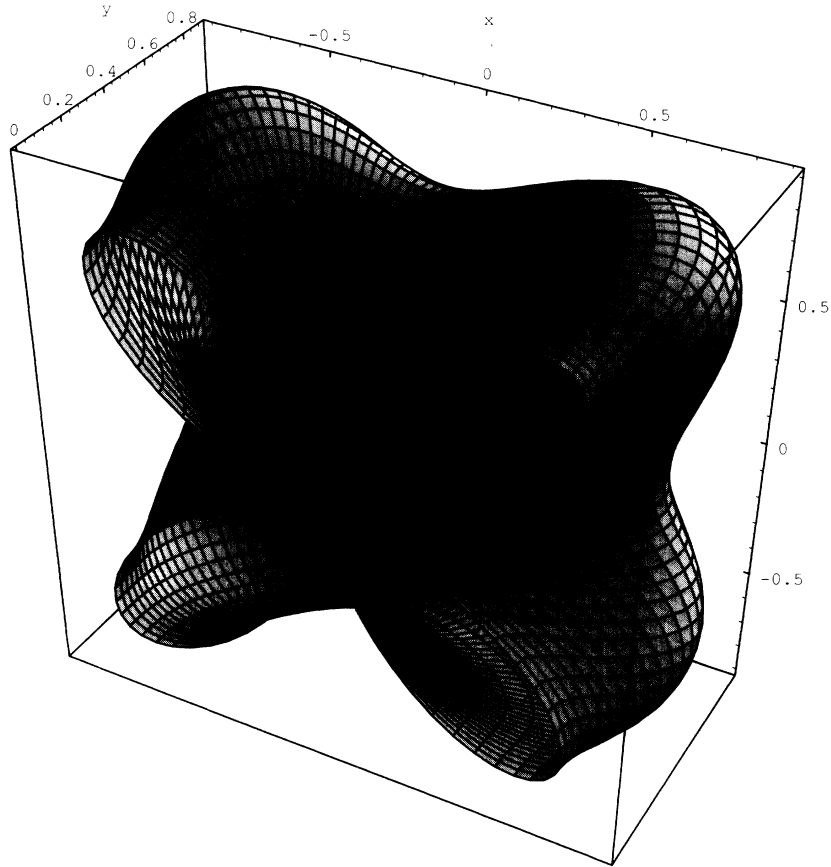


FIG. 6. Parametric plot of $\gamma(\phi, \theta)$ of Eq. (45) over half of the unit sphere. The surface shown is defined by the spherical polar coordinates $(\gamma(\phi, \theta), \phi, \theta)$. The function $\gamma(\phi, \theta)$ has a minimum value of 0 along the six $\langle 001 \rangle$ directions, and a maximum value of $4/3$ along the eight $\langle 111 \rangle$ directions.

and similarly for q_B . For cubic materials, the general form for q is^{51,16}

$$q(\hat{k}) = 1 - \frac{B}{C_{11} + \gamma(\hat{k})\Delta}, \quad (44)$$

where B is the bulk modulus, $\Delta = C_{44} - (C_{11} - C_{12})/2$ is the elastic anisotropy, and γ is a purely geometrical factor given by

$$\gamma(\hat{k}) = \gamma(\phi, \theta) = \sin^2(2\theta) + \sin^4(\theta) \sin^2(2\phi), \quad (45)$$

where ϕ and θ are spherical polar coordinates defined by $\mathbf{r} = [r \sin(\theta) \cos(\phi), r \sin(\theta) \sin(\phi), r \cos(\theta)]$. For the principal directions we have $\gamma[001] = 0$, $\gamma[011] = 1$, and $\gamma[111] = 4/3$, which is its maximum value. A parametric plot of $\gamma(\phi, \theta)$ is presented in Fig. 6. The minimum value of γ lies along the [001] direction and the maximum along the [111] direction.

D. Calculating $\Delta E_{\text{CS}}^{\text{eq}}(\hat{G}, x)$

From Eq. (42) we see that, if the elastic constants are known, only two calculations are needed [for $\Delta E_A(a_B)$ and $\Delta E_B(a_A)$] to determine $\Delta E_{\text{CS}}^{\text{eq}}(\hat{k}, x)$ for any binary system. We fit the form of Eq. (44) to calculations of $\Delta E_{\text{GaP}}^{\text{epi}}(\hat{k}, a_{\text{InP}})$ and $\Delta E_{\text{InP}}^{\text{epi}}(\hat{k}, a_{\text{GaP}})$ for $\hat{k} = [001]$ and $[011]$, using B/C_{11} and Δ/C_{11} as two fitting parameters. We do the same for InP. Note that in this procedure we do not use any values of $\Delta E_{\text{CS}}^{\text{eq}}(\hat{k}, x)$ as input. In particular, we need never perform calculations to find the minimum-energy substrate lattice constant a_{\perp}^{eq} , which would be an arduous task. Nonetheless, the elastic energy formula makes excellent predictions for the values of $\Delta E_{\text{CS}}^{\text{eq}}$. This is demonstrated in Fig. 7, where we plot the elastic energy predicted by Eq. (42), and the elastic energy calculated directly within the VFF model. (For the direct VFF calculations, the value of a_{\perp} is found by calculating the elastic energies for ten different values of the substrate lattice constant, performing a polynomial interpolation the elastic energy as a function of substrate lattice constant, and then minimizing the polynomial. This procedure is repeated for each direction and each value of x .) Equation (42) is seen to predict both the \hat{k} dependence and the x dependence correctly; the largest prediction error is < 0.25 meV/atom. This is an impressive performance when one considers that none of the constituent-strain energies shown in Fig. 7 were used to fit Eq. (42). Figure 8 shows a parametric plot of $\Delta E_{\text{CS}}^{\text{eq}}(\hat{k}, x = 1/2)$. The general features are the same as those of $\gamma(\hat{k})$, but less pronounced.

To use $\Delta E_{\text{CS}}^{\text{eq}}$ for our reciprocal-space strain expansion, we identify [see Eqs. (38) and (39)]

$$\begin{aligned} J_{\text{CS}}(\hat{k}, x) &= \frac{\Delta E_{\text{CS}}^{\text{eq}}(\hat{k}, x)}{4x(1-x)} \\ &= \frac{1}{4} \frac{q_A(\hat{k})q_B(\hat{k})\Delta E_A(a_B)\Delta E_B(a_A)}{(1-x)q_A(\hat{k})\Delta E_A(a_B) + xq_B(\hat{k})\Delta E_B(a_A)}, \end{aligned} \quad (46)$$

Elastic Theory for Constituent Strain

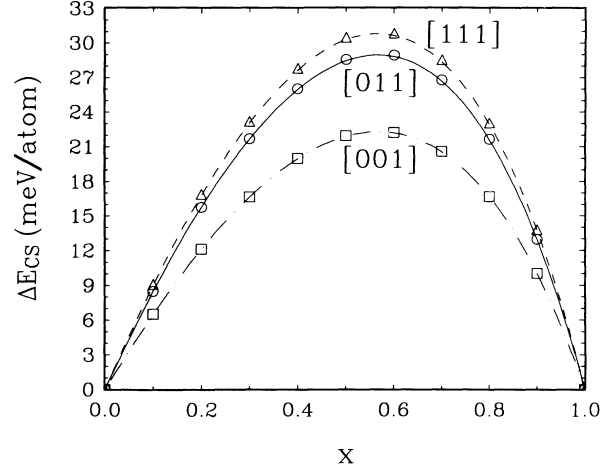


FIG. 7. Comparison of the elastic energy $\Delta E_{\text{CS}}^{\text{eq}}$ predicted by Eq. (42) with $\Delta E_{\text{CS}}^{\text{eq}}$ calculated directly by VFF for GaP/InP. The VFF results for the [001], [011], and [111] directions are indicated by squares, circles, and triangles, respectively. The elastic theory predictions for these three directions are indicated by dash-dotted, solid, and dashed lines, respectively.

where we now allow J_{CS} to depend on x . Equation (38) guarantees that this J_{CS} has the correct x dependence.

E. Working equations

We now summarize the practical use of this method with a set of step-by-step instructions for implementing the CE.

1. Calculate $\Delta E_{\text{CS}}^{\text{eq}}$ and J_{CS} .

- (a) Calculate the energies of cubic A at the lattice constant of cubic B [$\Delta E_A(a_B)$] and of B at the lattice constant of A [$\Delta E_B(a_A)$]. This can be done using first-principles total-energy methods.
- (b) Determine $q_A(\hat{k})$ and $q_B(\hat{k})$. This is done by calculating the energies of A constrained epitaxially to a_B in the plane perpendicular to \hat{k} and relaxed along the \hat{k} direction [$\Delta E_A^{\text{epi}}(\hat{k}, a_B)$], and similarly for B on A [$\Delta E_B^{\text{epi}}(\hat{k}, a_A)$]. This is repeated for two directions \hat{k} , and the values can then be used to solve for B/C_{11} and Δ/C_{11} for A using $q_A(\hat{k}) = \Delta E_A^{\text{epi}}(\hat{k}, a)/\Delta E_A(a)$, and similarly for B . $q(\hat{k}) = 1 - B/[C_{11} + \gamma(\hat{k})\Delta]$. The added work required to calculate $\Delta E_A(a_B)$, $\Delta E_B^{\text{epi}}(\hat{k}, a_B)$, and the like is quite small since each calculation is for the basic unit cell of the lattice, containing only one or two atoms.

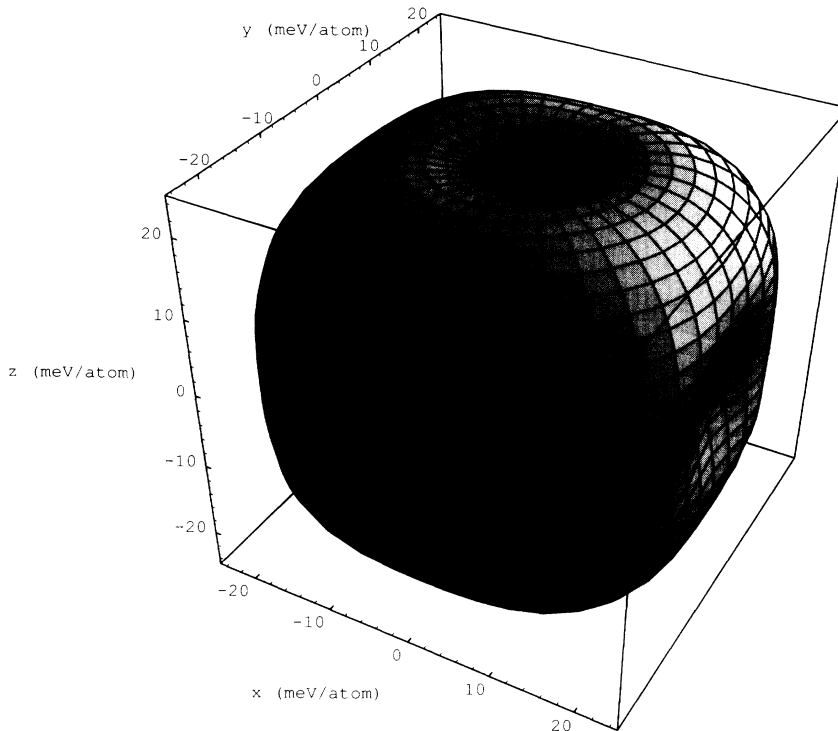


FIG. 8. Parametric plot of $\Delta E_{CS}^{\text{eq}}(\hat{k}, x = 1/2)$ from Eq. (42) for GaP/InP over the unit sphere. The surface shown is defined by the spherical polar coordinates $[\Delta E_{CS}^{\text{eq}}(\hat{k}, 1/2), \phi, \theta]$, in units of meV/atom.

(c) The working formula for $\Delta E_{CS}^{\text{eq}}$ is

$$\frac{1}{\Delta E_{CS}^{\text{eq}}(\hat{k}, x)} = \frac{1}{(1-x)q_A(\hat{k})\Delta E_A(a_B)} + \frac{1}{xq_B(\hat{k})\Delta E_B(a_A)}. \quad (47)$$

(d) The working formula for J_{CS} is $J_{CS}(\hat{k}, x) = \Delta E_{CS}^{\text{eq}}(\hat{k}, x)/[x(1-x)]$. See Eq. (46).

2. Choose a set of input structures $\{\sigma'\}$ and calculate the formation energies $E_{\text{direct}}(\sigma')$, using the same direct calculation technique that was used in step 1.

3. Find the interaction energies.

(a) Calculate $S(\mathbf{k}, \sigma')$ for all of the structures in the input set.

(b) Calculate $E'(\sigma') = E_{\text{direct}}(\sigma') - \sum_{\mathbf{k}} J_{CS}(\hat{k}) |S(\mathbf{k}, \sigma')|^2$.

(c) Choose a set of N_F nonpair interactions $\{F\}$ and a maximum number of pair interactions N_P .

(d) Vary $\{J_F\}$ $F = 1, N_F$ and $\{J_I\}$ $I = 1, N_P$ to minimize

$$\sum_{\sigma' \in s} w'_\sigma \left| E_{\text{direct}}(\sigma') - \sum_{\mathbf{k}} J_{CS}(\hat{k}, x) |S(\mathbf{k}, \sigma')|^2 - E'_{\text{CE}}(\sigma') \right|^2 + tM, \quad (48)$$

where M is given by Eq. (24), and t and λ are free parameters, with typical values $t = 1$ and $\lambda = 4$. E'_{CE} is defined by

$$E'_{\text{CE}}(\sigma') = N \sum_F' D_F J_F \bar{\Pi}_F(\sigma') + N \sum_{\mathbf{k}} J_{\text{SR}}(\mathbf{k}) |S(\mathbf{k}, \sigma')|^2, \quad (49)$$

$$\text{and } J_{\text{SR}}(\mathbf{k}) = \frac{1}{2} \sum_I^{N_P} J_{0,I} e^{i\mathbf{k} \cdot \mathbf{R}_I}.$$

4. The CE prediction for the $E_{\text{direct}}(\sigma)$ is

$$E_{\text{CE}}(\sigma) = E'_{\text{CE}}(\sigma) + N \sum_{\mathbf{k}} J_{CS}(\hat{k}, x) |S(\mathbf{k}, \sigma)|^2. \quad (50)$$

VII. RESULTS

We now present the results for the procedure outlined above. This CE differs from that of Fig. 3(c) only in the use of $E_{\text{ref}} = E_{CS}^{\text{eq}}(\hat{k}, x)$ in place of $E_{\text{ref}} = \Omega x(1-x)$. The

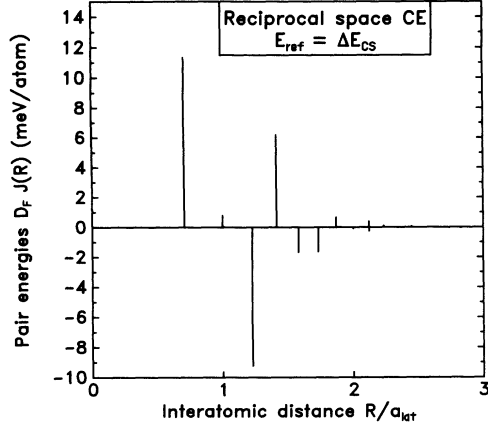


FIG. 9. Real-space pair interaction energies from the reciprocal-space fit using input set s_2 and $E_{\text{ref}} = \Delta E_{\text{CS}}^{\text{eq}}(\hat{k}, x)$.

prediction errors from this CE are shown in Fig. 3(d), and the real-space pair interactions and $J(\mathbf{k})$ (excluding J_{CS}) for this CE are shown in Figs. 9 and 10. [Figures 4 and 5 are the corresponding figures for the reciprocal-space fit with $E_{\text{ref}} = \Omega x(1-x)$.] Figure 11 shows that, as promised, the new fit solves the long-period superlattice problem demonstrated in Fig. 1. As before, we test the CE by predicting the energies of three sets of new structures, the long-period superlattices, swapped short-period structures, and $x \neq 1/2$ structures. These results are shown in the last line of Table III. Comparing parts (c) and (d) of Fig. 3, we find that the predictions for the long-period superlattices are, of course, greatly improved. But we also find better predictions for the swapped structures. This shows that the form that we use for J_{CS} is also helpful for *short-period* structures.

We can also use this CE to predict the energy of the random GaP/InP alloy. For the CE prediction of the random alloy energy for $x = 1/2$, we average $\Delta E_{\text{CS}}^{\text{eq}}(\hat{k}, x =$

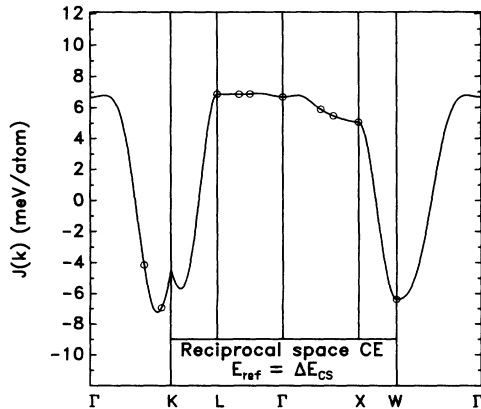


FIG. 10. $J(\mathbf{k})$ along the principal directions in the Brillouin zone for the same CE described in Fig. 9.

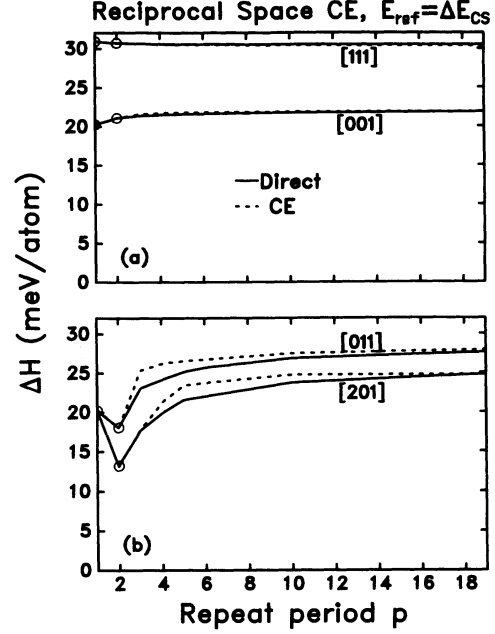


FIG. 11. Formation energies for GaP/InP superlattices as a function of repeat period p . Solid lines are results calculated with the VFF model. Dashed lines are results of a CE described in Fig. 9. The set of structures used to fit the interaction energies contains only structures with $p \leq 2$.

$1/2)$ over all solid angles. (This involves a slight approximation, as we should really be averaging over the first Brillouin zone.) We write

$$E_{\text{CE}}(\text{random}) = J_0 + \int \Delta E_{\text{CS}}^{\text{eq}}(\hat{k}, x) d\hat{k}. \quad (51)$$

The angular average of $\Delta E_{\text{CS}}^{\text{eq}}$ is 27.16 meV/atom and $J_0 = -6.47$ meV/atom. The CE predicted energy is 20.69 meV/atom, compared with 20.45 meV/atom from direct, 1000-atom simulations.⁵⁰

VIII. SUMMARY

We have demonstrated a reciprocal-space cluster expansion that is capable of making accurate predictions for systems that include atomic relaxations. We also show that lattice-mismatched superlattices with periods ≥ 3 undergo a correlated, long-ranged relaxation that cannot be correctly captured by a finite cluster expansion. To solve this problem, we derive a reciprocal-space cluster expansion for the elastic strain energy that has the correct limit for the long-period superlattices, and is well defined for nonsuperlattice structures. This reciprocal-space strain expansion is singular at $\mathbf{k} = 0$ and corresponds to an infinite set of pair interactions. The elastic strain expansion can be combined with a reciprocal-space expansion of the remaining short-ranged interactions, to yield a cluster expansion that is accurate for both short-period and long-period structures, as well as nonsuperlattice structures. As a bonus, expansions that include

the elastic strain energy also make more accurate predictions for short-period structures than those that do not. The method can predict the relaxed *energies* of arbitrary configurations, without having to calculate relaxed geometries or forces.

ACKNOWLEDGMENTS

We gratefully acknowledge many helpful discussions with S.-H. Wei. This work was supported in part by the Office of Energy Research, Materials Science Division, U.S. Department of Energy, under Grant No. DE-AC02-77-CH00178.

APPENDIX A: ELASTIC STRAIN ENERGY

We now derive the expression used for the constituent-strain energy [Eq. (42)]. Using harmonic elasticity theory,^{51,52} the energies of deforming *A* and *B* are

$$\Delta E_A(a) = \frac{9}{2} V_A B_A [\epsilon_A(a)]^2$$

and

$$(A1)$$

$$\Delta E_B(a) = \frac{9}{2} V_B B_B [\epsilon_B(a)]^2,$$

where $\Delta E_A(a)$ and $\Delta E_B(a)$ are the energies of cubic *A* and *B* at the lattice constant *a*, respectively, V_A and V_B are the equilibrium volumes of *A* and *B*, B is the bulk modulus, and ϵ is the strain. Inserting this into Eqs. (40) and (43) the elastic energy of an $A_{1-x}B_x$ superlattice in the direction \hat{k} is

$$\Delta E_{CS}^{\text{eq}}(\hat{k}, x) = (1-x)q_A(\hat{k})\frac{9}{2}V_A B_A \epsilon_A^2 + xq_B(\hat{k})\frac{9}{2}V_B B_B \epsilon_B^2,$$

(A2)

where q is an epitaxial relaxation parameter [Eq. (44)], and ϵ is the individual layer strain perpendicular to \hat{k} (which for simplicity we assume isotropic). Using Eulerian strain,

$$\epsilon_{A,B} = \frac{1}{2}(1 - a_{A,B}^2/a_{\perp}^2),$$

(A3)

and minimizing ΔE_{CS} with respect to a_{\perp} , the superlattice lattice constant parallel to the interfaces, we obtain the equilibrium value

$$a_{\perp}^2 = \frac{(1-x)q_A(\hat{k})V_A B_A a_A^4 + xq_B(\hat{k})V_B B_B a_B^4}{(1-x)q_A(\hat{k})V_A B_A a_A^2 + xq_B(\hat{k})V_B B_B a_B^2}. \quad (A4)$$

Inserting this value for a_{\perp} in Eq. (A3) gives the equilibrium constituent strains

$$\epsilon_A = -\frac{1}{2} \frac{xq_B(\hat{k})V_B B_B a_B^2 (a_A^2 - a_B^2)}{(1-x)q_A(\hat{k})V_A B_A a_A^4 + xq_B(\hat{k})V_B B_B a_B^4}$$

(A5)

for *A*, and

$$\epsilon_B = \frac{1}{2} \frac{(1-x)q_A(\hat{k})V_A B_A a_A^2 (a_A^2 - a_B^2)}{(1-x)q_A(\hat{k})V_A B_A a_A^4 + xq_B(\hat{k})V_B B_B a_B^4}$$

(A6)

for *B*, which inserted into Eq. (A2) gives

$$\Delta E_{CS}^{\text{eq}}(\hat{k}, x) = \frac{9}{8} x(1-x)q_A(\hat{k})q_B(\hat{k})V_A B_A V_B B_B \frac{(a_A^2 - a_B^2)^2}{(1-x)q_A(\hat{k})V_A B_A a_A^4 + xq_B(\hat{k})V_B B_B a_B^4}.$$

(A7)

Equation (A7) makes the $x(1-x)$ dependence of $\Delta E_{CS}^{\text{eq}}$ explicit and shows that J_2 [see Eq. (38)] is approximately x independent. Equation (A7) can be rewritten as

$$\frac{1}{\Delta E_{CS}^{\text{eq}}(\hat{k}, x)} = \frac{1}{(1-x)q_A(\hat{k})\Delta E_A(a_B)} + \frac{1}{xq_B(\hat{k})\Delta E_B(a_A)}.$$

(A8)

It turns out the Eq. (A8) is valid independently of the particular choice that was made for the strain in Eq. (A3).

¹I. M. Torrence, *Interatomic Potentials* (Academic, New York, 1972).

²S. M. Foiles, *Phys. Rev. B* **32**, 7685 (1985).

³P. C. Kelires and J. Tersoff, *Phys. Rev. Lett.* **63**, 1164 (1989).

⁴C. Domb, in *Phase Transitions and Critical Phenomena*, edited by C. Domb and H. S. Green (Academic, London, 1974), Vol. 3, p. 357.

⁵D. de Fontaine, in *Solid State Physics*, edited by H. Ehrenreich, F. Seitz, and D. Turnbull (Academic, New York, 1979), Vol. 34, p. 73.

⁶J. M. Sanchez and D. de Fontaine, in *Structure and Bonding in Crystals*, edited by M. O'Keefe and A. Navrotsky (Academic, New York, 1981), Vol. 2, p. 117.

⁷J. W. D. Connolly and A. R. Williams, *Phys. Rev. B* **27**,

5169 (1983).

⁸L.G. Ferreira, S.-H. Wei, and A. Zunger, *Phys. Rev. B* **40**, 3197 (1989).

⁹J. M. Sanchez, F. Ducastelle, and D. Gratias, *Physica A* **128**, 334 (1984).

¹⁰J. Kanamori and Y. Takehashi, *J. Phys. (Paris)* **38**, 274 (1977).

¹¹S.-H. Wei, L.G. Ferreira, and A. Zunger, *Phys. Rev. B* **41**, 8240 (1990).

¹²F. Ducastelle, *Order and Phase Stability in Alloys* (North-Holland, Amsterdam, 1991).

¹³R. Magri, J.E. Bernard, and A. Zunger, *Phys. Rev. B* **43**, 1593 (1991).

¹⁴R. Magri, S.-H. Wei, and A. Zunger, *Phys. Rev. B* **42**, 11388 (1990).

- ¹⁵A. E. Carlsson, Phys. Rev. B **35**, 4858 (1987).
- ¹⁶Z. W. Lu, S.-H. Wei, A. Zunger, S. Frota-Pessoa, and L.G. Ferreira, Phys. Rev. B **44**, 512 (1991).
- ¹⁷S. de Gironcoli, P. Giannozzi, and S. Baroni, Phys. Rev. Lett. **66**, 2116 (1991).
- ¹⁸A. G. Khachatryan, *Theory of Structural Transformations in Solids* (Wiley, New York, 1983), p. 459.
- ¹⁹Z. W. Lu, S.-H. Wei, and A. Zunger, Phys. Rev. Lett. **68**, 1961 (1992).
- ²⁰Z. W. Lu, S.-H. Wei, and A. Zunger, Phys. Rev. B **45**, 10314 (1992).
- ²¹B. L. Gyorffy and G.M. Stocks, Phys. Rev. Lett. **50**, 374 (1983).
- ²²F. Ducastelle and F. Gautier, J. Phys. F **6**, 2039 (1976).
- ²³M. Sluiter and P. E. A. Turchi, Phys. Rev. B **40**, 11 215 (1989).
- ²⁴C. Sigli and J. M. Sanchez, Acta Metall. **36**, 367 (1988).
- ²⁵D. D. Johnson, D. M. Nicholson, F. J. Pinski, B. L. Gyorffy, and G. M. Stocks, Phys. Rev. Lett. **56**, 2088 (1986).
- ²⁶R. Kikuchi, J. M. Sanchez, D. de Fontaine, and H. Yamaguchi, Acta Metall. **28**, 651 (1980).
- ²⁷J. M. Sanchez, J. R. Barefoot, R. N. Jarrett, and J. K. Tien, Acta Metall. **32**, 1519 (1984).
- ²⁸C. Sigli and J. M. Sanchez, Acta Metall. **33**, 1097 (1985).
- ²⁹L.G. Ferreira, A. A. Mbaye, and A. Zunger, Phys. Rev. B **37**, 10 547 (1988).
- ³⁰G. P. Srivastava, J. L. Martins, and A. Zunger, Phys. Rev. B **31**, 3561 (1985).
- ³¹K. Terakura, T. Oguchi, T. Mohri, and K. Watanabe, Phys. Rev. B **35**, 2169 (1987).
- ³²J. M. Sanchez, Solid State Commun. **65**, 527 (1988).
- ³³A. E. Carlsson, Phys. Rev. B **40**, 912 (1989).
- ³⁴W.H. Press, B.P. Flannery, S.A. Teukolsy, and W.T. Vetterling, *Numerical Recipes* (Cambridge University Press, Cambridge, 1986).
- ³⁵R. Magri and A. Zunger, Phys. Rev. B **44**, 8672 (1991).
- ³⁶P. N. Keating, Phys. Rev. **145**, 637 (1966).
- ³⁷R. M. Martin, Phys. Rev. B **1**, 4005 (1970).
- ³⁸S.-H. Wei and H. Krakauer, Phys. Rev. Lett. **55**, 1200 (1985).
- ³⁹J. Ihm, A. Zunger, and M.L. Cohen, J. Phys. C **12**, 4409 (1979).
- ⁴⁰R.G. Dandrea, J.E. Bernard, S.-H. Wei, and A. Zunger, Phys. Rev. Lett. **64**, 36 (1990).
- ⁴¹F. J. Pinski, B. Ginatempo, D. D. Johnson, J. B. Staunton, G. M. Stocks, and B. L. Gyorffy, Phys. Rev. Lett. **66**, 766 (1991).
- ⁴²J. C. Mikkelsen, Jr. and J. B. Boyce, Phys. Rev. Lett. **49**, 1412 (1982).
- ⁴³J.L. Martins and A. Zunger, Phys. Rev. B **30**, 6127 (1984).
- ⁴⁴P. Letardi, N. Motta, and A. Balzarotti, J. Phys. C **20**, 2583 (1991).
- ⁴⁵M. Ichimura and A. Sasaki, Phys. Rev. B **36**, 9694 (1987).
- ⁴⁶G. Renaud, N. Motta, F. Lancon, and M. Belakhovsky, Phys. Rev. B **38**, 5944 (1988).
- ⁴⁷P. E. A. Turchi, M. Sluiter, F. J. Pinski, D. D. Johnson, D. M. Nicholson, G. M. Stocks, and J. B. Staunton, Phys. Rev. Lett. **67**, 1779 (1991).
- ⁴⁸A. Sher, M. van Schilfgaarde, A.-B. Chen, and W. Chen, Phys. Rev. B **36**, 4279 (1987).
- ⁴⁹B. Chakraborty and Z. Xi, Phys. Rev. Lett. **68**, 2039 (1992).
- ⁵⁰J.E. Bernard (unpublished).
- ⁵¹S. Froyen, S.-H. Wei, and A. Zunger, Phys. Rev. B **38**, 10 124 (1988).
- ⁵²A. Zunger and D. M. Wood, J. Crystal Growth **98**, 1 (1989).

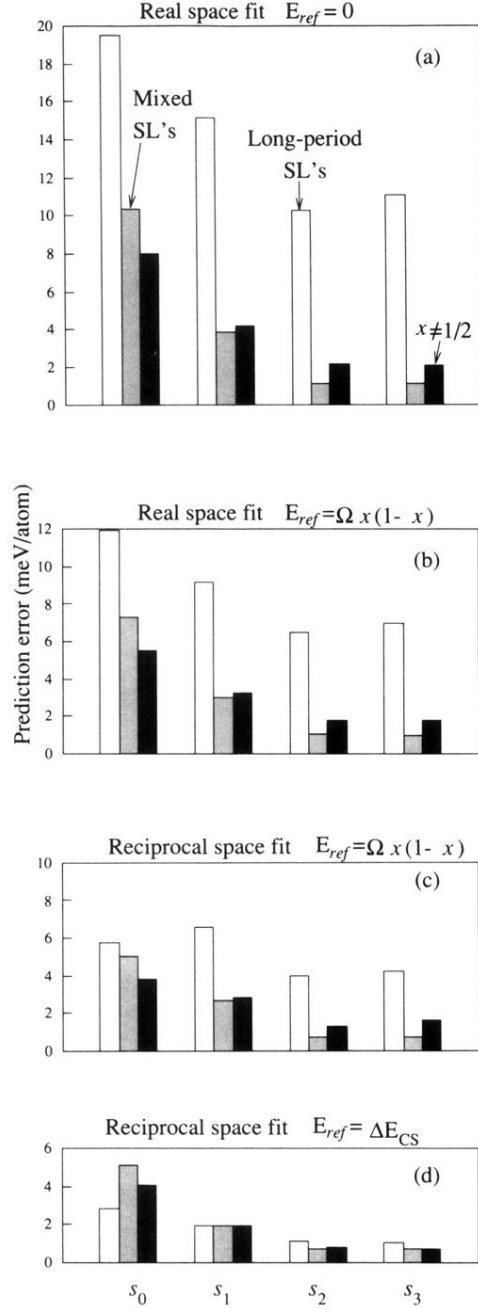


FIG. 3. Prediction errors for different CE's, in meV/atom. The CE is applied to $E - E_{ref}$ for four different fitting procedures: (a) Real-space fit with $E_{ref} = 0$ and $N_P \leq 7$. N_P is adjusted such that the number of figures is always less than or equal to the number of input structures. (b) Real-space fit with $E_{ref} = \Omega x(1-x)$ where Ω is treated as a fitting parameter and $N_P \leq 7$. (c) Reciprocal-space fit with $E_{ref} = \Omega x(1-x)$ and $N_P = 20$. (d) Reciprocal-space fit with $E_{ref} = \Delta E_{CS}$ and $N_P = 20$. Root-mean-square prediction errors (root-mean-square average of $E_{direct} - E_{CE}$) are shown separately for superlattices with $p > 3$ (open rectangles), superlattices with $p = 1, 2$ and atoms swapped across the interface (shaded rectangles), and structures with $x \neq 1/2$ (solid rectangles). Each CE is repeated using the input sets s_0 , s_1 , s_2 , and s_3 (defined in Sec. V C). Real-space fits have the scaling parameter $t = 0$, while reciprocal-space fits have $t = 1$ [Eq. (26)].

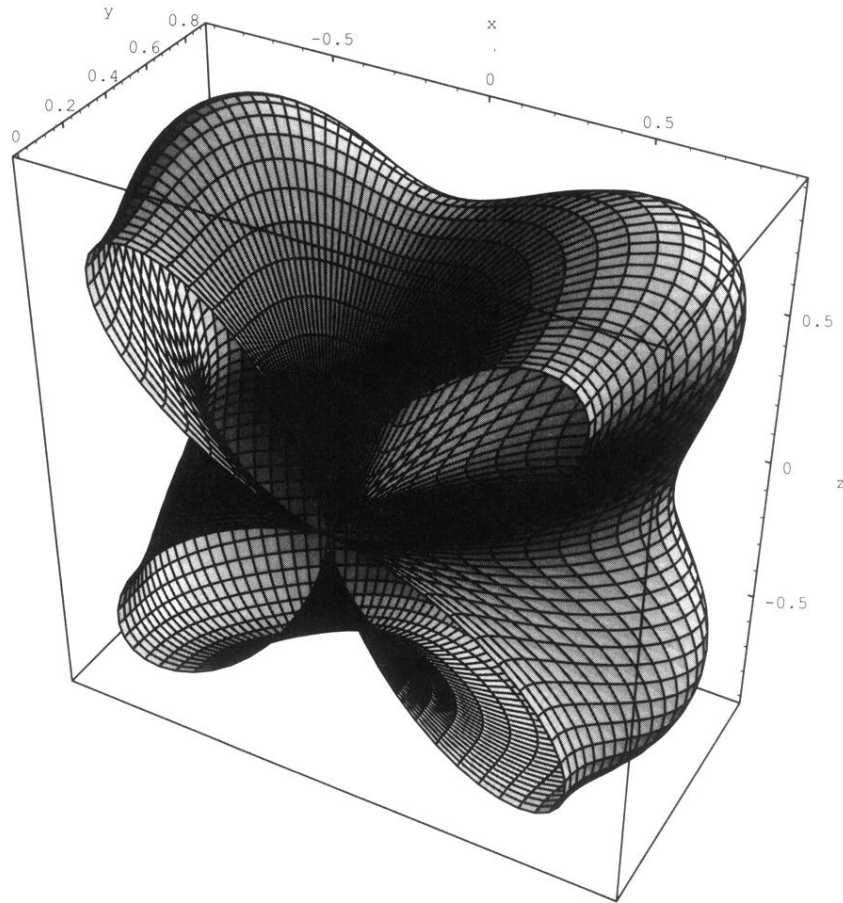


FIG. 6. Parametric plot of $\gamma(\phi, \theta)$ of Eq. (45) over half of the unit sphere. The surface shown is defined by the spherical polar coordinates $(\gamma(\phi, \theta), \phi, \theta)$. The function $\gamma(\phi, \theta)$ has a minimum value of 0 along the six $\langle 001 \rangle$ directions, and a maximum value of $4/3$ along the eight $\langle 111 \rangle$ directions.

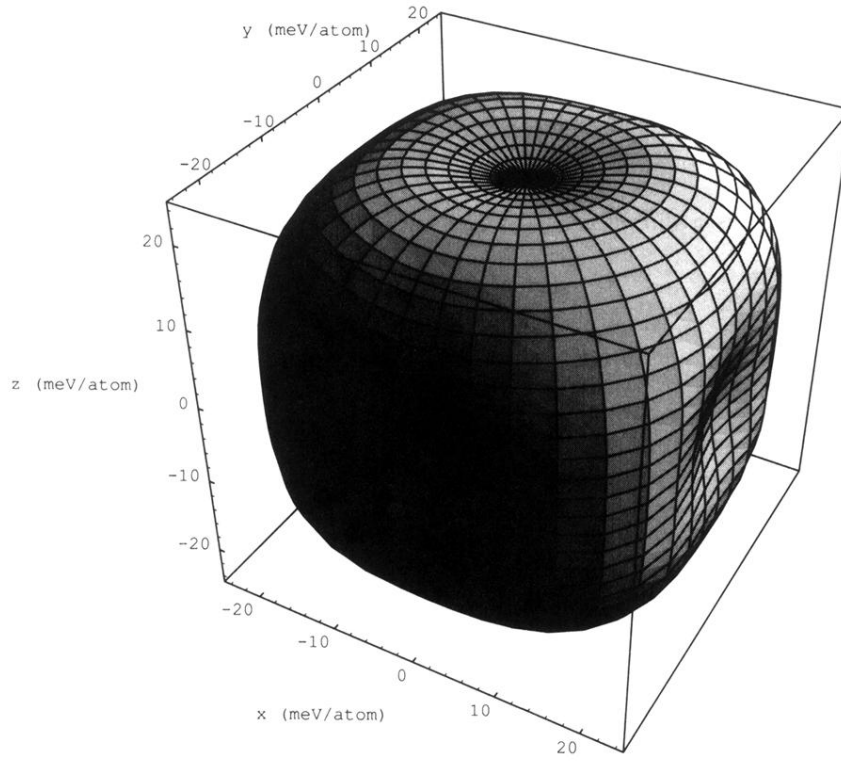


FIG. 8. Parametric plot of $\Delta E_{\text{CS}}^{\text{eq}}(\hat{k}, x = 1/2)$ from Eq. (42) for GaP/InP over the unit sphere. The surface shown is defined by the spherical polar coordinates $[\Delta E_{\text{CS}}^{\text{eq}}(\hat{k}, 1/2), \phi, \theta]$, in units of meV/atom.